

Coherent backscattering of light by an inhomogeneous cloud of cold atoms

Guillaume Labeyrie,¹ Dominique Delande,² Cord A. Müller,^{1,3} Christian Miniatura,¹ and Robin Kaiser¹

¹Laboratoire Ondes et Désordre, FRE 2302 du CNRS, 1361 route des Lucioles, 06560 Valbonne, France

²Laboratoire Kastler Brossel, Université Pierre et Marie Curie, Case 74, 4 place Jussieu, 75252 Paris, France

³Max-Planck-Institut für Physik komplexer Systeme, Nöthnitzer Strasse 38, D-01187 Dresden, Germany

(Received 7 October 2002; published 27 March 2003)

When a quiresonant laser beam illuminates an optically thick cloud of laser-cooled rubidium atoms, the average diffuse intensity reflected off the sample is enhanced in a narrow angular range around the direction of exact backscattering. This phenomenon is known as coherent backscattering (CBS). By detuning the laser from resonance, we are able to modify the light scattering mean-free path inside the sample and we record accordingly the variations of the CBS cone shape. We then compare the experimental data with theoretical calculations and Monte Carlo simulations including the effect of the light polarization and of the internal structure of the atoms. We confirm that the internal structure strongly affects the enhancement factor of the cone and we show that the unusual shape of the atomic medium—approximately a spherically-symmetric, Gaussian density profile—strongly affects the width and shape of the cone.

DOI: 10.1103/PhysRevA.67.033814

PACS number(s): 42.50.-p, 42.25.Dd, 32.80.Pj, 05.60.Gg

I. INTRODUCTION

Coherent backscattering (CBS) is an interference effect arising when a wave propagates and is multiply scattered inside a random medium. Its manifestation is an enhancement of the configuration-averaged diffuse intensity in a narrow angular range around exact backscattering, known as the CBS cone due to its distinctive shape [1]. This shape is given by the Fourier transform of the radial intensity distribution on the surface of the sample when illuminated by a pointlike source [2]. In a homogeneous semi-infinite medium, the width of the cone is known to be inversely proportional to the wave transport mean-free path ℓ^* in the sample [3]. For finite-size samples, the cone shape depends not only on the mean-free path but also on the sample geometry, and usually no analytical expression is available.

During the past decades, CBS has been thoroughly investigated experimentally on a variety of samples [4], mostly in the “slab” geometry. We have devised an experiment to study CBS of light on a sample of laser-cooled rubidium atoms [5,6]. This is an unusual situation, both because of the very peculiar properties of the atomic scatterers and of the distinctive geometry of the sample (spherical symmetry and quasi-Gaussian density profile). In previous publications [6–8], we have shown that the atomic Zeeman internal structure drastically reduces the contrast of the CBS interference, even in the helicity-preserving polarization channel. Our discussion of double scattering from a semi-infinite medium [7] already allowed for a qualitative understanding of the experimental data. The aim of the present article is to compare quantitatively our experimental data with Monte Carlo simulations taking into account the vector nature of light, the atomic internal structure and the inhomogeneous density of the scattering medium, with emphasis on the effect of the peculiar geometry used, which strongly affects the angular width of the CBS cone.

In Sec. II, we briefly recall the principle of the experiment. We describe in some detail the procedure to determine

the optical thickness of the sample, the most important experimental parameter for the comparison with the Monte Carlo simulations. The principle of the Monte Carlo simulations is described in detail in Sec. III. A theoretical discussion of the influence of the shape of the scattering medium on the CBS cone is presented in Sec. IV. Finally, we present in Sec. V the results of our Monte Carlo calculations, compare them with our theoretical predictions and the experimental results obtained on classical point dipole scatterers and on atomic scatterers.

II. EXPERIMENTAL SETUP

Our experimental setup has already been described in detail elsewhere [6], thus we just recall here its most important features. The whole signal acquisition procedure is time sequenced and repeated as long as necessary to get a good signal-to-noise ratio. First, during 20 ms, we trap Rb⁸⁵ atoms from a dilute vapor into a magneto-optical trap (MOT) using six large laser beams (diameter 2.8 cm, power 30 mW, wavelength $\lambda = 780$ nm) and a magnetic-field gradient of typically 10 G/cm (“bright” period). Then, during 5 ms, the MOT laser beams and magnetic gradient are turned off (“dark” period). During this period, the CBS probe laser beam is switched on (duration 1 ms), the CBS detection path is opened thanks to a mechanical chopper and the CBS signal is recorded on a cooled CCD camera. This “dark” period is short enough so that the cold atoms do not leave the trapping area and can be recaptured during the following “bright” period. A typical CBS image is obtained by integrating over several thousand cycles, corresponding to a total image acquisition duration of about 1 mn (effective signal acquisition duration about 2 s).

The probe laser beam is tuned on the $D2$ line $5S_{1/2} \rightarrow 5P_{3/2}$ of Rb⁸⁵ at $\lambda = 780$ nm and is quiresonant with the corresponding hyperfine ($J=3 \rightarrow J'=4$) transition (natural

linewidth $\Gamma/2\pi = 5.9$ MHz).¹ Since the other possible hyperfine transitions of the $D2$ line are far away from this transition (at least one order of magnitude at the Γ scale), multiple scattering is essentially driven by this unique and closed transition. However, the important degeneracy in the ground-state ($2J+1=7$ sublevels) allows both Rayleigh and degenerate Raman transitions between the different ground-state Zeeman sublevels. The amplitudes associated to direct and reverse scattering paths are strongly affected by the internal degeneracy, so that their interference gives a CBS cone much smaller than for point-dipole scatterers [7,8]. Especially, the so-called enhancement factor, which measures the ratio of the diffuse intensity at exact backscattering to the “background” diffuse intensity (close to the backward direction, but outside the CBS cone), is typically of the order of 1.05 to 1.2, instead of close to 2 for point-dipole scatterers [9].

The polarizations of the incident and backscattered lights play an important role. The most common choices are either linear or circular polarizations. This leads to four different polarization channels: $lin\parallel lin$ where both the incoming and outgoing photons are linearly polarized along the same axes, $lin\perp lin$ where they are linearly polarized along orthogonal axes, $h\parallel h$ where they are both circularly polarized with the same helicity (because they propagate in opposite directions, they have opposite polarizations) and $h\perp h$ where they are circularly polarized with opposite helicities, i.e., same polarization. Large enhancement factors are observed for point dipole scatterers in the parallel channels and especially exactly 2 in the $h\parallel h$ channel [9,10]. For atomic scatterers, the largest enhancement factor on the $3\rightarrow 4$ transition is measured on the contrary in the $h\perp h$ channel [6,8].

Since we aim at a quantitative comparison with the numerical simulations, we need to carefully characterize our cloud of cold atoms. Two measurements are performed to this end. First, we determine the cloud shape by imaging on the CCD the fluorescence induced by a detuned probe beam. We use two viewing angles at 90° to have access to the cloud density profiles in the three spatial dimensions. It is important to detune the probe beam from resonance so that light-atoms interaction occurs in the single scattering regime. This ensures a uniform illumination of the atomic cloud. The cloud shape is most of the time slightly anisotropic, depending on the alignment of the trapping beams. However, the experimental results presented in this paper were obtained with a quasi-isotropic cloud whose full width at half maximum (FWHM) dimensions are $3.7\times 4.1\times 4.0$ mm (see Fig. 1). The density profiles are close to a Gaussian, although somewhat sharper, especially at the entrance of the light in the medium. This has a small, yet measurable effect on the properties of the CBS cone, see Sec. V C.

Second, we measure the optical thickness at the center of the atomic cloud [11]. A small and weak probe laser beam (diameter 1 mm) with central angular frequency ω is sent

¹In conventional spectroscopic notations, the total atomic angular momenta are noted using F 's and not J 's. We have deliberately chosen to ignore this prescription and to stick to the notations used in the theoretical papers [7,8].

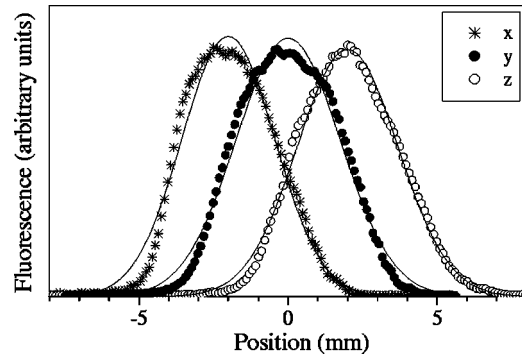


FIG. 1. Density profiles of the cold rubidium cloud used in the CBS experiment. The profiles are obtained by illuminating the atomic cloud by a far-detuned probe beam and by imaging the induced fluorescence signal at two orthogonal viewing angles on a CCD camera. The profiles have been shifted for the sake of clarity. Axis z defines the propagation axis of the CBS probe beam, whereas axis y corresponds to the polarization axis of the probe light (in the linear channels). The atomic cloud is quasiisotropic with quasiGaussian profiles (the solid lines correspond to the Gaussian fits) of FWHM $3.7\times 4.1\times 4.0$ mm (x,y,z).

through the center of the trap and the so-called “coherent” transmitted mode (selected using two diaphragms separated by 2 m) intensity is recorded as a function of the probe detuning $\delta = (\omega - \omega_{at})$. Scanning the laser detuning around the atomic resonance modifies the atomic response and accordingly the depletion of the “coherent” beam since the scattering cross section is [8]

$$\sigma(\delta) \equiv \sigma = \frac{\sigma_{res}}{1 + (2\delta/\Gamma)^2} \quad (1)$$

with σ_{res} the on-resonance scattering cross section. The cloud transmission curve $T(\delta)$ is the monochromatic transmission curve $T_0(\delta) = \exp[-b(\delta)]$ (Lambert-Beer’s law) convolved by the probe laser frequency spectrum (a Lorentzian curve of width ≈ 2 MHz). The monochromatic optical thickness $b(\delta)$ is readily given by

$$b(\delta) \equiv b = \frac{b_{res}}{1 + (2\delta/\Gamma)^2}, \quad (2)$$

where b_{res} is the on-resonance optical thickness.

From the measured data, we extract the b_{res} value [11]. For a Gaussian density profile of rms -radius r_0 in the direction of propagation of the probe, the monochromatic optical thickness is readily given by $b = \sqrt{2\pi}n_0\sigma r_0 = \sqrt{2\pi}r_0/\ell$, where n_0 is the spatial density at the trap center. The quantity $\ell(\delta) \equiv \ell = 1/n_0\sigma$ is the scattering mean-free path at the center of the trap. Usually, the relevant length scale for CBS is the *transport* mean-free path ℓ^* . It is related to the scattering mean-free path ℓ (as obtained by optical thickness

measurement²) by the expression : $\ell^* = \ell / (1 - \langle \cos \theta \rangle)$, where the term $\langle \cos \theta \rangle$ represents the forward-backward asymmetry of the radiation pattern. For a symmetric radiation pattern (e.g., point-dipole scatterer), $\langle \cos \theta \rangle = 0$ yielding $\ell^* = \ell$. The same property is valid for atomic scatterers [8]. The procedure described above allows the measurement of large optical thicknesses, without systematic errors caused by the probe laser spectrum [11]. In the experiment reported here, the maximum on-resonance optical thickness was $b_{\text{res}} = 33$. From the b_{res} (transmission) and r_0 (fluorescence imaging) values, one obtains the on-resonance mean-free-path ℓ_{res} at the center of the cloud. Assuming a uniform population distribution among Zeeman sublevels and no optical pumping, the on-resonance scattering cross section is [8]

$$\sigma_{\text{res}} = \frac{2J'+1}{3(2J+1)} \frac{3\lambda^2}{2\pi}, \quad (3)$$

where the first factor is unity for point-dipole scatterers which are equivalent to atomic scatterers on a $J=0 \rightarrow J'=1$ transition. We can also compute the peak density n and the total number of atoms \mathcal{N} in the cloud. We obtain typical values of $\mathcal{N} = 4 \times 10^9$ atoms and $n_0 = 6 \times 10^{10} \text{ cm}^{-3}$ in our sample, yielding $\ell_{\text{res}} \approx 135 \mu\text{m}$. We also measured the temperature of the atomic cloud by the time-of-flight technique to be in the 100 μK range (residual *rms*-velocity spread about 10 cm s^{-1}).

The on-resonance mean-free path at the center of the sample is much larger than the wavelength. We are thus in the dilute regime, where $k\ell_{\text{res}} \gg 1$. The typical angular width of the CBS cone is of the order of 0.5 to 1 mrad, well above the resolution limit of the apparatus (0.1 mrad).

The CBS probe laser beam is not a true plane wave but rather a Gaussian laser beam. The waist of the laser beam is approximately located on the atomic cloud (so that the wave fronts are planar) and the FWHM of the beam intensity is 8.3 mm (beam waist 7 mm). Additionally, a diaphragm with diameter 8 mm is added on the laser beam. The goal is that all atoms of the atomic cloud are exposed to the same incoming field. Deviations from uniform illumination are known to be responsible for modifications of the CBS cone shape, which can be taken into account in the numerical Monte Carlo calculations, see Sec. III D.

Once the atomic cloud parameters are determined, the optical thickness can be simply varied by adjusting the detuning δ of the CBS probe beam from exact resonance. We here report results where the detuning is varied from 0 (exact resonance; optical thickness 33) to 4Γ (optical thickness 0.5). This makes it possible, with a fixed geometry, to cover the whole range from a thin to a very thick medium, thus exploring various regimes of multiple scattering.

III. MONTE CARLO CALCULATIONS

Except in rare cases, it is impossible to compute exactly the properties of the CBS cone. The few situations where the results are known in closed form are the scattering of a scalar wave by point scatterers in a semi-infinite medium or very thick slab [12] (see Ref. [13] for a review) or the scattering of an electromagnetic vector wave by point-dipole scatterers (also known as Rayleigh scatterers) [14,15]. It should also be mentioned that, for quasideviant scattering by an atom on a $J \rightarrow J'$ transition, the double scattering contribution from a semi-infinite medium is known exactly [8]. The case of a slab of finite optical thickness and constant density could also be calculated using the same techniques. For atomic scatterers, the structure of the individual scattering event is slightly more complicated than for classical point-dipole scatterers, but it is not unlikely that the methods used in Ref. [15] could be extended to calculate the CBS cone for a uniform semi-infinite medium. Such an extension is however not straightforward. At a more fundamental level, the fact that the atomic density in a magneto-optical trap is not uniform, makes it very difficult—if not impossible—to compute exactly the cone properties.

The CBS cone arises in the diffuse intensity, averaged over the disordered external and internal degrees of freedom of the scatterers. We choose to perform the average over the positions of the scatterers with a Monte Carlo method and to use an internal analytical average by employing the average atomic scattering vertex [8,16]. This method is flexible, as it makes it possible to compute the quantities of interest for an arbitrary atomic transition and—this is the most important point—for an arbitrary spatial repartition of the scatterers. It also allows us to take into account some rather small, yet not negligible effects, such as the nonuniform incoming intensity sent on the sample (because a Gaussian laser beam is used). All calculations and simulations in this paper are performed for a *monochromatic* probe laser beam. This approximation seems well justified since the probe beam frequency spectrum is sufficiently narrow in the experiment (roughly one third of the atomic natural linewidth). Indeed, as we shall see in Sec. V C, the width and enhancement factor of the atomic CBS cone are only weakly dependent on the optical thickness and thus on the laser linewidth.

We first describe the method in the simplest case, a medium with the shape of a slab and a uniform density of scatterers which isotropically scatter a scalar plane wave perpendicular to the entrance of the slab. We then show how the calculation can be extended to a medium of arbitrary shape and density. We discuss the complications arising when a vector (electromagnetic) wave is considered, and finally show how the calculation can be extended to atomic scatterers. Our goal here is not to go in every detail or give mathematical proofs of the correctness of the method, but rather to give the important ingredients and hints to enable the reader to reproduce our calculations.

A. Scalar wave in a uniform slab of point scatterers

In this simple case, the first basic ingredient is the scattering amplitude or its modulus square, the differential cross-section, which is isotropic and thus can be written as

²Optical thickness measurements actually define the extinction length of the sample. When absorption is negligible, which is the case here, it simply reduces to the scattering mean-free-path ℓ .

$$\frac{d\sigma}{d\Omega}(\Omega) = \frac{\sigma}{4\pi}, \quad (4)$$

where σ is the total scattering cross section. The second basic ingredient is the average amplitude propagator (inside the medium) between two consecutive scattering events,

$$G(k, \mathbf{r}) = -\frac{1}{4\pi r} \exp(ikr) \exp\left(-\frac{r}{2\ell}\right), \quad (5)$$

where k is the wave vector (inside the medium) and ℓ the mean-free path. As we are interested in very dilute media, such that the (uniform) density of scatterers n is small

$$\frac{n}{k^3} \ll 1, \quad (6)$$

the real part of the wave vector—at lowest order—is identical inside and outside the medium. Also, the mean-free path is simply related to the total cross section by

$$\ell = \frac{1}{n\sigma}. \quad (7)$$

The bistatic coefficient is a dimensionless coefficient which expresses how much of the incoming intensity is scattered in any direction. It is related to the scattering cross section of the whole medium by

$$\gamma(\mathbf{k}_{\text{in}}, \mathbf{k}_{\text{out}}) = \frac{4\pi}{A} \left\langle \frac{d\Sigma}{d\Omega}(\mathbf{k}_{\text{in}} \rightarrow \mathbf{k}_{\text{out}}) \right\rangle, \quad (8)$$

where \mathbf{k}_{in} and \mathbf{k}_{out} are the incoming and outgoing wave vectors, A is the transverse area of the medium and $d\Sigma/d\Omega$ the scattering cross section by this area of the medium (for an infinite medium, it reduces to the cross section per unit of area). In this expression, the brackets $\langle \dots \rangle$ denote an ensemble averaging over all positions of the scatterers, in the so-called thermodynamic limit where the number of individual scatterers as well as the size of the system tend to infinity, at constant density of scatterers.

The cross-section $\langle (d\Sigma/d\Omega)(\mathbf{k}_{\text{in}} \rightarrow \mathbf{k}_{\text{out}}) \rangle$ involves multiple scattering events at various orders. For a dilute medium, it is possible to expand the total cross section using a diagrammatic approach and to determine, order by order, which diagrams survive the configuration averaging and those give the dominant contributions. We refer the reader to Refs. [3,17] for details. For our purpose, it is sufficient to know that the diffuse intensity is given by the sum of the so-called “ladder” contributions—which vary smoothly in the vicinity of the backscattered direction—and the “crossed” contributions—which vary rapidly around the exact backscattered direction and describe the CBS cone—to the bistatic coefficient,

$$\gamma = \gamma_L + \gamma_C. \quad (9)$$

Each contribution can be expanded in a multiple scattering series

$$\gamma_L = \sum_{N=1}^{\infty} \gamma_L^{(N)}, \quad (10)$$

$$\gamma_C = \sum_{N=2}^{\infty} \gamma_C^{(N)}. \quad (11)$$

Note that there is no crossed contribution for single scattering $N=1$.

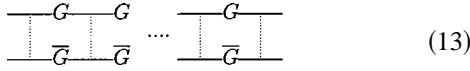
For simplicity, we assume that both the in-going and out-going wave vectors are perpendicular to the slab. The case of arbitrary incident and reflected angles can be treated along the same lines, at the price of slightly more complicated expressions. At scattering order N , the “ladder” bistatic coefficient can be written as (assuming that $\mathbf{k}_{\text{in}} = -\mathbf{k}_{\text{out}}$ is along the z axis and that the boundary of the medium is at $z=0$):

$$\begin{aligned} \gamma_L^{(N)} &= \frac{4\pi}{A} n^N \int d\mathbf{r}_1 d\mathbf{r}_2 \dots d\mathbf{r}_N \exp\left(-\frac{z_1}{\ell}\right) \\ &\times \left(\frac{d\sigma}{d\Omega}\right)_1 [16\pi^2 G(k, \mathbf{r}_{12}) \bar{G}(k, \mathbf{r}_{12})] \\ &\times \left(\frac{d\sigma}{d\Omega}\right)_2 \dots \left(\frac{d\sigma}{d\Omega}\right)_{N-1} \\ &\times [16\pi^2 G(k, \mathbf{r}_{N-1,N}) \bar{G}(k, \mathbf{r}_{N-1,N})] \\ &\times \left(\frac{d\sigma}{d\Omega}\right)_N \exp\left(-\frac{z_N}{\ell}\right), \end{aligned} \quad (12)$$

where $\mathbf{r}_{ij} = \mathbf{r}_j - \mathbf{r}_i$ and the integral over the scatterers’ positions has to be taken over the whole medium. The terms $\exp(-z_1/\ell)$ and $\exp(-z_N/\ell)$ represent the attenuation of respectively, the incoming wave between the entrance in the medium and the first scattering event and the outgoing wave between the last scattering event and the exit of the medium.³ The differential cross-sections represent the successive scattering events while Green’s functions represent the propagation in the effective medium in between scatterers. Note that the phase $\exp(ikr)$ in Green’s function cancels out between G and its complex conjugate \bar{G} so that the bistatic coefficient is positive. There is no interference effect in this bistatic coefficient: it is actually associated with a classical transport equation. This expression is also valid if the differential cross section is not isotropic.

The integrand can be represented by the following diagram:

³The ladder contribution is here calculated at backscattering. Since the direction of observation appears only in the last term $(d\sigma/d\Omega)_N \exp(-z_N/\ell)$, the ladder contribution is a very smooth function of the scattering angle.



where the vertical dotted lines represent the scattering events, each vertex on the lower and upper horizontal lines represents a scattering amplitude, the horizontal lines with G and \bar{G} represent the amplitude Green function joining two consecutive scatterers, and the initial and final incomplete horizontal lines represent the exponential attenuation before the first and after the last scattering events, respectively.

For single scattering from a slab of optical thickness b , the integration over \mathbf{r}_1 is trivial and one gets

$$\gamma_L^{(1)} = \frac{1 - \exp(-2b)}{2} \quad (14)$$

for isotropic point scatterers.

The form of Eq. (12) is not suitable for a Monte Carlo configuration averaging because of the exponential attenuation of the Green function over a mean-free path. It is more convenient to use relative displacements from one scatterer to the next one. For example, for isotropic point scatterers, the double-scattering ladder bistatic coefficient can be rewritten, using Eq. (5) as

$$\gamma_L^{(2)} = \frac{n^2 \sigma^2}{4\pi A} \int d\mathbf{r}_1 d\mathbf{r}_2 \frac{\exp\{-(z_1 + z_2 + r_{12})/\ell\}}{r_{12}^2}. \quad (15)$$

Performing the change of variables $(\mathbf{r}_1, \mathbf{r}_2) \rightarrow (\mathbf{r}_1, \mathbf{r}_{12})$, the integral over the transverse coordinates of the first scatterer is trivial. Then, using spherical coordinates for the relative distance \mathbf{r}_{12} and rescaling all positions with respect to the mean-free path $\ell = 1/n\sigma$, we get

$$\gamma_L^{(2)} = \int dz_1 dr_{12} \frac{d\Omega_{12}}{4\pi} \exp\{-(z_1 + z_2 + r_{12})\}. \quad (16)$$

The structure of this integral is clear: once the position of the first scatterer is chosen, the integral over the position of the second scatterer can be easily evaluated by the Monte Carlo method: it is in a random direction from the initial scatterer, with an exponential distribution of the distance from it, and must be still present in the medium, i.e., z_2 must be positive and smaller than the optical thickness of the slab (otherwise, the contribution vanishes). Once this averaging over r_{12} and Ω_{12} is performed, one is left with a single integral over z_1 , which also has an exponential weight. This integral can also be performed using a Monte Carlo method.⁴ For the triple-scattering contribution, the strategy is the same, with the choice of the initial position of the first scatterer, then the random choice of the position of the second scatterer with the *ad hoc* distribution of their relative distance, and similarly the random choice of the third scatterer once the position of the second one is known.

⁴In the simple case of a semi-infinite medium, the integral for double scattering can be easily performed analytically, yielding $\gamma_L^{(2)} = \ln 2/2$.

A crucial point—which saves a lot of computing resources—is to remark that, when calculating the triple-scattering contribution, the double scattering can be obtained at almost no extra cost. Indeed, the (random) choice of the positions of the various scatterers is done successively starting from the first one, then determining the position of the second one, then the position of the third one. Once the first two scatterers have been chosen, the contribution of this configuration to the double-scattering bistatic coefficient is straightforward from Eq. (15). Thus, a scattering path with N scattering events can be used for all orders of scattering from 1 to N (this is the “partial photon” method discussed in Appendix C of Ref. [4]). This trick essentially saves a factor N in the calculation, where N is the typical scattering order of a path in the medium. In the diffusion approximation, N is of the order of the square of the optical thickness of the medium. With the maximum optical thickness in the experiment one finds $N \approx 10^3$, so that the saving is substantial. The whole procedure actually relies on the “ladder” structure of the diagram (13): the diagram at scattering order N is obtained from the diagram at order $(N-1)$ by simply adding an additional rung to the ladder.

More precisely, the algorithm is the following one.

(1) Choose randomly the depth of the first scatterer according to an exponential distribution.

(2) Calculate the contribution to single scattering.

(3) Choose randomly the position of the next scatterer in a random direction from the previous scatterer at a distance given by an exponential distribution. If the chosen position is outside the medium, stop the current scattering path and initiate a new one (go to step 1). If not, compute the contribution to the ladder bistatic coefficient (i.e., multiply by $\exp(-z_N/\ell)$, where z_N is the depth of the current scatterer).

(4) Go to step 3 in order to compute the contribution at next order.

By restarting the full procedure as soon as the position of a scatterer is outside the medium, we ensure automatically the correct weights of the various scattering orders.

The “crossed” contribution, which gives the CBS cone, can be calculated along the same lines. Indeed, for isotropic scatterers and a scalar wave, its contribution to the bistatic coefficient at scattering order N is

$$\begin{aligned} \gamma_C^{(N)} = & \frac{4\pi}{A} n^N \int d\mathbf{r}_1 d\mathbf{r}_2 \cdots d\mathbf{r}_N \exp\left(-\frac{z_1}{\ell}\right) \\ & \times \left(\frac{d\sigma}{d\Omega}\right)_1 [16\pi^2 G(k, \mathbf{r}_{12}) \bar{G}(k, \mathbf{r}_{12})] \\ & \times \left(\frac{d\sigma}{d\Omega}\right)_2 \cdots \left(\frac{d\sigma}{d\Omega}\right)_{N-1} \\ & \times [16\pi^2 G(k, \mathbf{r}_{N-1,N}) \bar{G}(k, \mathbf{r}_{N-1,N})] \left(\frac{d\sigma}{d\Omega}\right)_N \\ & \times \exp\left(-\frac{z_N}{\ell}\right) \times \cos[(\mathbf{k}_{\text{in}} + \mathbf{k}_{\text{out}}) \cdot (\mathbf{r}_N - \mathbf{r}_1)]. \quad (17) \end{aligned}$$

The corresponding ‘‘crossed diagram’’ is, for double scattering,


(18)

Because the scattering process has time-reversal symmetry, it is possible to unfold this diagram—so that what enters on the left side is now the incoming field on the upper branch, but the outgoing field in the lower branch—and recover the ladder diagram. The price to pay is that all phase factors do not cancel any longer, yielding the additional term $\cos[(\mathbf{k}_{\text{in}} + \mathbf{k}_{\text{out}}) \cdot (\mathbf{r}_N - \mathbf{r}_1)]$, with respect to the ladder contribution.

Exactly the same diagrams and the same scattering paths can be used for computing the ladder and crossed contributions. The only difference is in the single scattering term, which is absent in the crossed contribution. Such a procedure automatically ensures the equality of the ladder and crossed contributions in the backscattered direction $\mathbf{k}_{\text{out}} = -\mathbf{k}_{\text{in}}$, where the cosine is unity. Consequently, the enhancement factor in the backward direction is equal to 2 at all scattering orders, except of course for single scattering, where the crossed contribution does not exist. Away from backscattering, the cosine term in the crossed bistatic coefficient must be configuration averaged. When $\|\mathbf{k}_{\text{in}} + \mathbf{k}_{\text{out}}\|$ is much larger than $1/\ell$, the cosine oscillates rapidly and configuration averaging causes the crossed contribution to vanish. This is why the crossed contribution describes the CBS peak centered around exact backscattering with an angular width of the order of $1/k\ell$.

B. Scalar wave in a uniform medium with arbitrary geometry

In our experiments, the scatterers are not uniformly distributed in a slab. The Monte Carlo calculation can handle this complication easily. If the medium has a uniform density, the propagator is not modified (as long as the photon does not leave the medium). Hence, only the configuration averaging is affected. If the system does not have a translational invariance perpendicularly to the incoming direction, the bistatic coefficient defined by Eq. (8) is no longer useful. Yet, the diffuse intensity reflected off the medium can be determined using the same techniques: we calculate the average total cross section $\langle (d\Sigma/d\Omega)(\mathbf{k}_{\text{in}} \rightarrow \mathbf{k}_{\text{out}}) \rangle$ using an expansion in successive scattering orders and calculating the configuration average through successive random choices of the positions of the scatterers until the medium is left.⁵

C. Scalar wave in a medium with arbitrary geometry and arbitrary density

In a real experiment, the density of scatterers is not uniform. As the cloud of atomic scatterers is produced in a

magneto-optical trap (switched off when CBS is recorded), the density of scatterers is usually maximal at the center of the trap. As a rough approximation, the density of scatterers is close to an isotropic Gaussian distribution

$$n(\mathbf{r}) = n_0 \exp\left(-\frac{\mathbf{r}^2}{2r_0^2}\right), \quad (19)$$

where n_0 is the density at the center of the trap and r_0 the *rms*-radius of the trap. The maximum optical thickness of the sample is obtained along a diameter

$$b = \sqrt{2\pi} n_0 \sigma r_0. \quad (20)$$

The main difference with the preceding paragraphs is that the mean-free path is no longer a constant, but varies across the sample. It reads

$$\ell(\mathbf{r}) = \frac{1}{\sigma n(\mathbf{r})} = \ell \exp\left(\frac{\mathbf{r}^2}{2r_0^2}\right), \quad (21)$$

where ℓ is the *minimum* mean-free path, at the center of the sample,

$$\ell = \frac{1}{n_0 \sigma} = \frac{\sqrt{2\pi} r_0}{b}. \quad (22)$$

More complicated situations can be described as well. For example, it often happens that—because of the parameters of the MOT—the atomic cloud is not isotropic. In such a case, the density of scatterers is usually well approximated by an anisotropic Gaussian distribution

$$n(\mathbf{r}) = n_0 \exp\left(-\frac{x^2}{2x_0^2} - \frac{y^2}{2y_0^2} - \frac{z^2}{2z_0^2}\right). \quad (23)$$

Numerical calculations turn out to show that this may significantly affect the CBS cone shape. For example, the agreement between the experimental CBS cone for the Strontium atoms and the numerical calculation in Ref. [18] required taking this effect into account.

Because the mean-free path is no longer constant, it is obvious that the propagator in the effective medium is also affected. The attenuation factor, instead of decreasing exponentially, has simply to be replaced by the cumulative decrease along the path. The average amplitude Green function (which depends now on both the initial and final points) becomes

$$G(k, \mathbf{r}_1, \mathbf{r}_2) = -\frac{1}{4\pi r_{12}} \exp(ikr_{12}) \exp\left[-\frac{\sigma}{2} \int_0^{r_{12}} n(\mathbf{r}_1 + s\mathbf{u}_{12}) ds\right], \quad (24)$$

where $\mathbf{u}_{12} = (\mathbf{r}_2 - \mathbf{r}_1)/r_{12}$ is the unit vector joining the initial and final points. In this expression, we assumed that the

⁵If we assume that the medium is convex—which is always the case in our experiments—once a photon leaves the medium, it never reenters it. Nonconvex media can also be treated if one carefully checks whether the photon has really escaped or not.

wave-vector k does not vary inside the medium, an approximation which would break down at high density of scatterers.

The inclusion of expression (24) in the above expressions for the bistatic coefficient (or the back-reflected diffuse intensity) is rather straightforward. In a Monte Carlo calculation, once the density of scatterers $n(\mathbf{r})$ is known, it is enough to choose randomly the direction of propagation after the N th scattering event and the distance to the next scatterer according to the Green function, Eq. (24), using for example a rejection method [19]. The additional cost induced by the rejection method is almost negligible for the choice of the direction of propagation (because the cross section is not far from uniform). It is significantly more expensive for the choice of the next scattering event along a path, and slows down the calculation by up to one order of magnitude. On the other hand, it is extremely flexible. For special cases (e.g. Gaussian density of scatterers), an analytic expression in terms of the error function exists for the integral in Eq. (24), and can be used for choosing the position of the next scatterer, reducing the total cost.

D. Nonuniform incoming laser beam

Additional complications can be easily introduced in the Monte Carlo calculation. For example, in our experiment the incoming beam is not exactly a plane wave but a Gaussian beam of large waist (7 mm). The Monte Carlo calculation can be amended by weighting properly each contribution. The weight is simply proportional to the amplitudes of the fields entering the various diagrams (from the left). Thus, the ladder contribution can be written as

$$L = \sum_p \int d\mathbf{r} d\Delta\mathbf{r} |a_p(\mathbf{r}, \Delta\mathbf{r}) \mathcal{E}(\mathbf{r})|^2, \quad (25)$$

where $\mathcal{E}(\mathbf{r})$ represents the incoming field at position \mathbf{r} on the entrance plane of the medium (or any plane before the entrance in the medium) and $a_p(\mathbf{r}, \Delta\mathbf{r})$ is the contribution (calculated as described above) of a scattering path labeled by p which starts at position \mathbf{r} on the entrance plane and exits at $\mathbf{r} + \Delta\mathbf{r}$. Similarly, the crossed contribution can be written as

$$C(\Delta\mathbf{k}) = \sum_p \int d\mathbf{r} d\Delta\mathbf{r} a_p(\mathbf{r}, \Delta\mathbf{r}) a_{\tilde{p}}(\mathbf{r}, \Delta\mathbf{r}) \times \mathcal{E}(\mathbf{r}) \bar{\mathcal{E}}(\mathbf{r} + \Delta\mathbf{r}) \exp(i\Delta\mathbf{k} \cdot \Delta\mathbf{r}) \quad (26)$$

with $\Delta\mathbf{k} = \mathbf{k}_{\text{in}} + \mathbf{k}_{\text{out}}$. Here \tilde{p} is the reverse scattering path associated to p (same scatterers visited but in opposite order) and $a_{\tilde{p}}$ denotes its amplitude.

For the ladder contribution, it is thus the square on the incoming field, i.e., the incident intensity which weights the various contributions. For the crossed contribution, the weight is proportional to the product of the fields at the initial and final points of the scattering path. In general, this breaks the equality of the ladder and crossed contributions at exact backscattering. Thus, a nonuniform incoming field will generally lead to a reduction of the enhancement factor. If

the waist of the incoming beam is much larger than the mean-free path of the light in the medium, then the laser intensity is locally constant over a multiple scattering path and the imbalance between the two fields will be negligible: the CBS cone will not be affected. On the contrary, a too narrow incoming beam will broaden the CBS peak. If the medium is statistically invariant by translation perpendicular to the incoming direction (as for example the slab medium and the Gaussian slab discussed below), the amplitude a_p associated with a path depends only on $\Delta\mathbf{r}$, but not on the initial point \mathbf{r} itself. Under these conditions, the calculation of the ladder term is trivial⁶ as it appears as the product of the ladder term for an infinite medium (the quantity discussed in the previous section) multiplied by the total intensity $I_0 = \int d\mathbf{r} |\mathcal{E}(\mathbf{r})|^2$. The structure of the crossed term is slightly more complicated. It appears as the Fourier transform with respect to $\Delta\mathbf{r}$ of the product of $a_p(\Delta\mathbf{r}) a_{\tilde{p}}(\Delta\mathbf{r})$ by

$$g(\Delta\mathbf{r}) = \int d\mathbf{r} \mathcal{E}(\mathbf{r}) \bar{\mathcal{E}}(\mathbf{r} + \Delta\mathbf{r}). \quad (27)$$

The Fourier transform of a product being the convolution of the Fourier transforms, it appears that the crossed term is the convolution of the Fourier transform of $a_p(\Delta\mathbf{r}) a_{\tilde{p}}(\Delta\mathbf{r})$ by the Fourier transform of g . The first Fourier transform is nothing but the crossed term C_0 for the infinite medium (the quantity discussed above). The Fourier transform of g is the modulus square of the Fourier transform of the field, i.e., $I(\Delta\mathbf{k}) = |\hat{\mathcal{E}}(\Delta\mathbf{k})|^2$. It has a simple physical interpretation: it is the angular distribution of the intensity of the incoming beam. Finally, one gets the simple convolution

$$C(\Delta\mathbf{k}) = \int C_0(\mathbf{k}) I(\Delta\mathbf{k} - \mathbf{k}) d\mathbf{k}. \quad (28)$$

Once the CBS cone shape is calculated for an incoming plane wave, it is obtained for a finite incoming beam through a (two-dimensional) convolution. Obviously, this decreases the enhancement factor at the center of the cone and increases its width. Although the previous derivation did not consider the polarization of the light, it is of course also valid for vector waves. It should however be emphasized that it is valid only for a medium which is transversely invariant, and thus fails for a sphere or a Gaussian sphere.

An additional complication is that some diaphragms are present in the experiment on the incoming beam and on the optical device which collects the scattered photons. This is straightforwardly taken into account in the Monte Carlo calculation by simply cutting the contributions of all scattering paths which hit a diaphragm. Altogether, the Monte Carlo

⁶In this derivation of the ladder term (and the derivation of the crossed term below), we assume that the incoming laser beam has an angular width (in radians) much smaller than unity, so that all terms, except the phase of the interference, can be considered as constant and evaluated at normal incidence. This will fail for a point source near the surface for example.

calculation for a nonuniform medium is not much more expensive than for a uniform medium.

E. Electromagnetic wave and point-dipole scatterers

When an electromagnetic wave is considered, the situation is slightly more complicated, because the polarization of the wave has to be taken into account. This affects both the elementary scattering event and the propagation in the average medium. The scattering cross section depends of course on the polarization of the incident and scattered light as well as on the relative orientation of the incoming and outgoing directions. For point-dipole scatterers—classical scatterers much smaller than the wavelength and having no internal structure—everything is known in closed analytic form [20]. The differential cross section writes

$$\frac{d\sigma}{d\Omega}(\mathbf{k}_{in}, \boldsymbol{\epsilon}_{in} \rightarrow \mathbf{k}_{out}, \boldsymbol{\epsilon}_{out}) = \frac{3\sigma}{8\pi} |\bar{\boldsymbol{\epsilon}}_{in} \cdot \boldsymbol{\epsilon}_{out}|^2, \quad (29)$$

where $\boldsymbol{\epsilon}_{in}, \boldsymbol{\epsilon}_{out}$ denote the incoming and outgoing polarizations, respectively orthogonal to \mathbf{k}_{in} and \mathbf{k}_{out} .

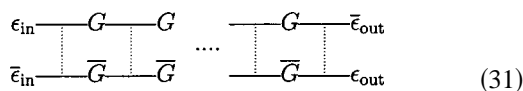
The average amplitude propagator in the (uniform) medium reads [8]

$$G(k, \mathbf{r}) = -\frac{\Delta_{\mathbf{r}}}{4\pi r} \exp(ikr) \exp\left(-\frac{r}{2\ell}\right), \quad (30)$$

where $\Delta_{\mathbf{r}}$ is the projector perpendicular to \mathbf{r} acting in the space of polarizations: $(\Delta_{\mathbf{r}})_{ij} = \delta_{ij} - r_i r_j / r^2$ and the mean-free path ℓ is again given by Eq. (7).

The calculation of the bistatic coefficient is similar to the calculation for scalar waves. The only difference is that the polarizations of the incoming, outgoing, and intermediate photons as well as of the scattering vertex must be taken into account. Special care is needed when considering the polarization state of scattered photons. Indeed, given a multiple scattering path, the contributions of the possible polarizations of the photon between two consecutive scatterers must be taken into account. For long paths, the number of contributions increases very rapidly. However, the average amplitude propagator is the same for all polarizations, which means that they all are attenuated with the same mean-free path.⁷ It is thus possible using a given multiple scattering path to sum exactly the various contributions having different intermediate polarizations, simply giving the $\Delta_{\mathbf{r}}$ operator in the Green function, Eq. (30).

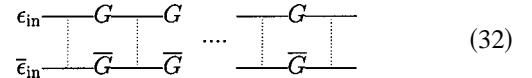
The situation is different for the ladder contributions and the crossed contributions. Indeed, the diagram associated with the ladder contribution is



$$\begin{array}{c} \epsilon_{in} \text{---} G \text{---} G \text{---} \\ \vdots \quad \quad \quad \vdots \\ \bar{\epsilon}_{in} \text{---} \bar{G} \text{---} \bar{G} \text{---} \\ \vdots \quad \quad \quad \vdots \end{array} \dots \begin{array}{c} \text{---} G \text{---} \bar{\epsilon}_{out} \\ \vdots \quad \quad \quad \vdots \\ \text{---} \bar{G} \text{---} \epsilon_{out} \\ \vdots \quad \quad \quad \vdots \end{array} \quad (31)$$

⁷In contrast with the intensity whose different polarization modes decay with different characteristic lengths, see, for example, M. J. Stephen and G. Cwilich, Phys. Rev. B **34**, 7564 (1986).

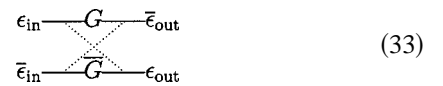
where, now, the scattering vertex by each scatterer is a quantity that depends on the four polarization vectors: 2 incoming vectors on the upper and lower horizontal lines (left side) and 2 outgoing vectors (right side). In this diagram, both the incoming field and its complex conjugate are scattered by the same scatterer: this results in the square modulus of the scattering amplitude, i.e., the scattering cross section. Thus, expressions like Eq. (12) can be used at the price of some book keeping of polarizations. Another difference with the case of scalar waves discussed above is that the differential cross section is no longer isotropic, which means that all scattering directions are not equally probable. We have used two different methods: either choose randomly the scattering direction at each scattering event and weight the contribution by the probability of the event (proportional to the differential cross section) or choose directly the scattering direction with a probability distribution matching the differential cross section. We have checked that both methods give the same results, although the second one is more accurate, as the integrand in the Monte Carlo integration is constant. Like for scalar waves, it is possible to use a given scattering path at order N to compute contributions at all orders between 1 and N . Indeed, the basic object which has to be propagated is the following diagram:



$$\begin{array}{c} \epsilon_{in} \text{---} G \text{---} G \text{---} \dots \text{---} G \text{---} \\ \vdots \quad \quad \quad \vdots \quad \quad \quad \vdots \quad \quad \quad \vdots \\ \bar{\epsilon}_{in} \text{---} \bar{G} \text{---} \bar{G} \text{---} \dots \text{---} \bar{G} \text{---} \end{array} \quad (32)$$

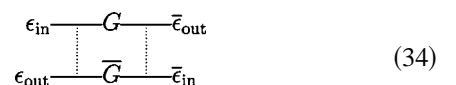
where the final polarizations (on the right side) are not specified. This object is a polarization tensor with $3 \times 3 = 9$ components. In order to get the contribution to the bistatic coefficient at order N , it is enough to contract this tensor with the tensor $\boldsymbol{\epsilon}_{out} \otimes \bar{\boldsymbol{\epsilon}}_{out}$ to obtain a real positive number. The polarization tensor at next order $N+1$ is obtained again by adding one rung to the ladder, i.e., choosing conveniently the relative position of the next scatterer (which takes into account the scattering cross section and the exponential attenuation of Green's function) and multiplying the polarization tensor at order N by the tensor $\Delta_{\mathbf{r}_{N,N+1}} \otimes \Delta_{\mathbf{r}_{N,N+1}}$ (which takes into account the polarization part of Green's function). For point-dipole scatterers, the scattering vertex is the direct product of the direct and conjugated amplitude [cf. Eq. (29)]. Thus, the polarization tensor is—at any step—a direct product of the type $\boldsymbol{\epsilon} \otimes \bar{\boldsymbol{\epsilon}}$, so that one needs only to propagate the three components of a vector, instead of the nine components on the tensor. Physically, $\boldsymbol{\epsilon}$ is nothing but the polarization of the photon after N scattering events.

For the crossed contributions, the situation is more complicated. Indeed, the diagram is (represented here for double scattering)



$$\begin{array}{c} \epsilon_{in} \text{---} G \text{---} \bar{\epsilon}_{out} \\ \vdots \quad \quad \quad \vdots \\ \bar{\epsilon}_{in} \text{---} \bar{G} \text{---} \epsilon_{out} \\ \vdots \quad \quad \quad \vdots \end{array} \quad (33)$$

Because of time reversal invariance, the scattering vertex is not affected when the lower line is returned. It is thus possible to unfold the diagram completely,



$$\begin{array}{c} \epsilon_{in} \text{---} G \text{---} \bar{\epsilon}_{in} \\ \vdots \quad \quad \quad \vdots \\ \epsilon_{out} \text{---} \bar{G} \text{---} \bar{\epsilon}_{out} \\ \vdots \quad \quad \quad \vdots \end{array} \quad (34)$$

It thus appears that the incoming and outgoing fields are scattered along the same multiple-scattering path. In the $lin\parallel lin$ channel, ϵ_{in} and ϵ_{out} are real and equal; in the $h\parallel h$ channel, they are complex conjugate. In this case, again the product of the two scattering amplitudes is nothing but the cross section, so that the situation is essentially similar to the scattering of scalar waves. The crossed bistatic coefficient at exact back scattering is equal to the ladder bistatic coefficient—except for single scattering—and a large enhancement factor is expected. This is indeed what is experimentally observed in the “parallel” channels $lin\parallel lin$ and $h\parallel h$ [4]. In addition, in the $h\parallel h$ channel, the single-scattering cross section in the backward direction vanishes, leading to a factor 2 enhancement for the CBS cone.

In the “perpendicular” channels $lin\perp lin$ and $h\perp h$, the incoming and outgoing polarizations are not complex conjugate, and the propagation is slightly more complicated. Another polarization tensor,

$$\begin{array}{c} \epsilon_{in} \text{---} G \text{---} G \\ \vdots \quad \quad \quad \vdots \\ \epsilon_{out} \text{---} \bar{G} \text{---} \bar{G} \end{array} \quad \dots \quad \begin{array}{c} \text{---} G \text{---} \\ \vdots \quad \quad \quad \vdots \\ \text{---} \bar{G} \text{---} \end{array} \quad (35)$$

has to be propagated in the Monte Carlo calculation. It is no longer the cross section that appears in expressions like Eq. (12), but products of two scattering amplitudes [8]. However, the Monte Carlo method can still be used, by choosing randomly the position of the next scattering event (with an exponential distribution of the distance in a uniform medium) and the relative direction of scattering, taking into account the weight due to the product of various scattering amplitudes through the polarization tensor. Again, this polarization tensor is a direct product of two vectors, which makes its propagation slightly simpler.

For a medium with a nonuniform density of scatterers, the method developed for scalar waves in Sec. III C can be easily used, at the price of modifying the amplitude Green function. As the latter does not depend on the choice of polarization, the extension is straightforward.

F. Electromagnetic wave and atomic scatterers

When the individual scatterer has some internal structure, the situation is *much* more complicated. We consider here the case of an atom in a well-defined hyperfine level (angular-momentum J) exposed to a light quasisonant with a dipole transition to another hyperfine level with angular-momentum J' (with the usual selection rule $|J' - J| \leq 1$). When it scatters the incoming light, the atom may stay in the same Zeeman sublevel—this is a Rayleigh transition—or change its magnetic quantum number—this is a degenerate Raman transition. In both cases, if recoil and Doppler effects are negligible (which one expects to be the case for our cold atomic cloud), the scattered photon has the same frequency as the incoming photon: the scattering is elastic.

The scattering amplitude by a single atom depends on the initial and final Zeeman sublevels, on the scattering direction

and on the incident and scattered polarizations. As the atoms produced in a MOT are not in a well-defined internal state, but rather in a statistical mixture of Zeeman states, the calculation of the bistatic coefficient requires, in addition to the usual configuration averaging, an averaging over the internal state of the atom. A first solution could be to perform the latter averaging using a brute force Monte Carlo approach. The individual scattering amplitudes are well known (see Ref. [8] for explicit expressions). However, the average amplitude Green’s function is extremely complicated if no assumption is made on the internal state of the atom. The simplest assumption is that the atoms are completely depolarized, i.e., described by a scalar density matrix in their ground state. Then, as shown in Ref. [8], the average amplitude Green’s function takes the same form, Eq. (30), than for point-dipole scatterers. This assumption on the internal state is likely to be correct for atoms produced in a MOT. When exposed to a polarized incoming beam, it could be that some optical pumping takes place. We have used weak probe beams in the experiment in order to minimize optical pumping.

As the scalar density matrix hypothesis is needed to get a simple amplitude Green’s function in the medium, it can also be used to simplify the calculation of the bistatic coefficient. In Ref. [8], it has been shown that averaging over the internal state can be performed analytically for each individual scattering event. The average differential cross section now reads

$$\left\langle \frac{d\sigma}{d\Omega} \right\rangle = \frac{3\sigma}{8\pi} (w_1 |\bar{\epsilon}_{in} \cdot \epsilon_{out}|^2 + w_2 |\epsilon_{in} \cdot \epsilon_{out}|^2 + w_3), \quad (36)$$

where the weights are $w_1 = 23/56$, $w_2 = -3/14$, $w_3 = 15/56$ for the present case $J = 3 \rightarrow J' = 4$. The single-scattering vertex thus contains all three possible contractions between the polarization vectors and will be represented by a vertical ribbon instead of a single dotted line. The contribution to the ladder bistatic coefficient can be written (for simplicity, we show the diagram for double scattering) as

$$\begin{array}{c} \epsilon_{in} \text{---} G \text{---} \bar{\epsilon}_{out} \\ \vdots \quad \quad \quad \vdots \\ \bar{\epsilon}_{in} \text{---} \bar{G} \text{---} \epsilon_{out} \end{array} \quad (37)$$

In complete similarity with point-dipole scatterers discussed above, we can propagate in the Monte Carlo calculation a polarization tensor which is “initialized” (on the left side) with the direct product $\epsilon_{in} \otimes \bar{\epsilon}_{in}$. How this tensor is affected by a scattering event is described in detail in Refs. [8,16]. The only difference with point-dipole scatterers is that the polarization tensor cannot any longer be written as a direct product of two vectors. Hence, the 9 (complex) components of the polarization tensor have to be propagated during the Monte Carlo calculation. At each step, the contribution to the ladder bistatic coefficient is obtained by contracting the polarization tensor with $\epsilon_{out} \otimes \bar{\epsilon}_{out}$.

For the crossed contribution, the diagram (for double scattering) is

$$\begin{array}{c} \epsilon_{in} \text{---} G \text{---} \bar{\epsilon}_{out} \\ \text{---} \bar{G} \text{---} \epsilon_{out} \\ \bar{\epsilon}_{in} \text{---} G \text{---} \epsilon_{out} \\ \text{---} \bar{G} \text{---} \bar{\epsilon}_{out} \end{array} \quad (38)$$

The unfolding of the diagram is slightly more complicated. Indeed, the expression of the scattering vertex is such that it is no longer invariant when the lower line is returned. Diagrammatically, the returned crossed contribution

$$\begin{array}{c}
 \epsilon_{\text{in}} \text{---} \overbrace{\hspace{1.5cm}}^G \text{---} \bar{\epsilon}_{\text{out}} \\
 \epsilon_{\text{out}} \text{---} \underbrace{\hspace{1.5cm}}_{\bar{G}} \text{---} \bar{\epsilon}_{\text{in}}
 \end{array} \quad (39)$$

is *not* equal to

$$\begin{array}{c}
 \epsilon_{\text{in}} \text{---} \overbrace{\hspace{1.5cm}}^G \text{---} \bar{\epsilon}_{\text{out}} \\
 \epsilon_{\text{out}} \text{---} \underbrace{\hspace{1.5cm}}_{\bar{G}} \text{---} \bar{\epsilon}_{\text{in}}
 \end{array} \quad (40)$$

However, as the structure of the scattering vertex is known exactly, the propagation of another polarization tensor for the crossed diagrams is easily handled in the Monte Carlo calculation through the substitution $w_2 \leftrightarrow w_3$ [8]. Altogether, the extra cost to be paid for atomic scatterers is rather modest. Note that, even for parallel polarization channels, the complication introduced by the atomic structure breaks the equality of the ladder and crossed contributions at exact backscattering. This is why enhancement factors smaller than 2 (and usually much smaller than 2) are observed. The simplest case of a $J=0 \rightarrow J'=1$ transition is an exception: because the ground state is not degenerate, the atom actually behaves like a classical point-dipole scatterer (the scattering vertex is the same as $w_1=1$ and $w_2=w_3=0$) and a large enhancement factor in the $h||h$ channel is observed [18].

The extension to nonuniform media follows exactly the same lines than for electromagnetic field and point-dipole scatterers.

IV. INFLUENCE OF THE SHAPE OF THE SCATTERING MEDIUM

While experiments on multiple scattering are often using scattering media with simple shapes (the simplest case being a semi-infinite medium with uniform density), this is difficult with cold atoms. Indeed cooling and trapping techniques provide finite-size atomic samples with nonuniform density distributions. As a first approximation, the atomic cloud density in our MOT is described by a Gaussian density (isotropic or anisotropic). This has important consequences for the multiply scattered light in general and the CBS cone in particular. Some of the effects (nonexhaustive list) are as following.

(1) The mean-free path of the photons is not uniform across the medium. It is maximum at the center of the cloud. Because the angular width of the CBS cone is inversely proportional to the mean-free path, this effect is likely to influence strongly the CBS cone's shape and width.

(2) Because the medium is finite in the transverse direction, photons can more easily escape the medium. Compared to a slab with the same optical thickness, it is thus expected that the effect of high-scattering orders will be smaller for an atomic cloud.

(3) If the incoming laser beam has a transverse width comparable to or larger than the cloud size (which is the case in the experiment), the photons which are far off the axis of the atomic cloud feel a very small optical thickness and will be mainly scattered once. Thus, the role of single

scattering—and more generally of low-order scattering—will be largely enhanced.

(4) Photons, which are off the axis of the atomic cloud do not enter the medium perpendicularly, which may affect the intensity scattered backward. Considering the rather weak dependence on the initial incident angle for a semi-infinite medium [13], this effect is expected to be small.

It is not *a priori* obvious which effect(s) will dominate. In order to clarify this issue, we have performed several Monte Carlo calculations with the following geometries:

Slab. Slab medium with uniform density,

$$n(\mathbf{r}) = n_0 \quad \text{for } 0 \leq z \leq r_0; \quad 0 \text{ otherwise.} \quad (41)$$

The optical thickness is $b = n_0 \sigma r_0$.

Gaussian slab. Slab medium with a nonuniform Gaussian density,

$$n(\mathbf{r}) = n_0 \exp\left(-\frac{z^2}{2r_0^2}\right). \quad (42)$$

The optical thickness is $b = \sqrt{2\pi} n_0 \sigma r_0$.

Sphere. Sphere uniformly filled with scatterers,

$$n(\mathbf{r}) = n_0 \quad \text{for } r \leq r_0; \quad 0 \text{ otherwise.} \quad (43)$$

The maximal optical thickness (for $x=y=0$) is $b = 2n_0 \sigma r_0$.

Gaussian sphere. Isotropic Gaussian density of scatterers,

$$n(\mathbf{r}) = n_0 \exp\left(-\frac{r^2}{2r_0^2}\right). \quad (44)$$

The maximal optical thickness (for $x=y=0$) is $b = \sqrt{2\pi} n_0 \sigma r_0$.

In all cases, we will assume that the maximum density of scatterers n_0 is fixed, so that the minimum mean-free-path ℓ (at the center of the medium) is also fixed. We will also compare different geometries for a fixed optical thickness b of the sample, adjusting r_0 accordingly. For the sphere and the Gaussian sphere, the optical thickness is measured along the diameter, where it is maximum.

The Gaussian slab will be sensitive to the spatial variations of the mean-free path, but not to the other effects discussed above. On the contrary, the sphere will be sensitive to the transverse effects but keeping a constant mean-free path. The Gaussian sphere—more or less the experimental medium—will show a mixture of both types of effects.

A. Multiple scattering by a Gaussian slab

In this section, we show that, at *exact* backscattering, the total bistatic coefficient for a Gaussian slab is *exactly* equal to the total bistatic coefficient for a slab with the same optical thickness. An even stronger result is established: at each scattering order N , the ladder bistatic coefficient $\gamma_L^{(N)}$ is identical for the uniform slab and the Gaussian slab; the same property is valid for the crossed bistatic coefficient $\gamma_C^{(N)}$ at exact backscattering. This is a very general result, valid for

scalar as well as electromagnetic waves, in the latter case for point-dipole scatterers and for atomic scatterers. Also, the precise shape of the density of scatterers does not matter, the only important point being that it has a translational invariance in the (x, y) plane perpendicular to the incoming beam. As far as we know, such a property, although quite simple, has not been previously noticed.

For simplicity, we prove this equality for scalar waves and isotropic point scatterers and for double scattering. The extension to more complicated cases is straightforward.

We start from Eq. (12), using the amplitude Green's function (24) for an inhomogeneous medium. We obtain

$$\gamma_L^{(2)} = \frac{\sigma^2}{4\pi A} \int d\mathbf{r}_1 d\mathbf{r}_2 n(\mathbf{r}_1) n(\mathbf{r}_2) \frac{1}{r_{12}^2} \exp\left\{-\sigma \left[\int_{-\infty}^{z_1} n(z) dz + \int_{-\infty}^{z_2} n(z) dz + \int_0^{r_{12}} n(\mathbf{r}_1 + s\mathbf{u}_{12}) ds \right]\right\}. \quad (45)$$

The translational invariance in the (x, y) makes it possible to perform trivially the integral over x_1 and y_1 , leaving a four-dimensional integral over z_1 and the three components of \mathbf{r}_{12} . For the latter, we will use spherical coordinates for the relative distance r_{12} and $\Omega_{12} = (\theta_{12}, \phi_{12})$.

The key point is then to remark that this expression essentially depends on the density of scatterers $n(z)$ integrated between successive z coordinates of the scatterers (and similar contributions for the incoming and outgoing paths). It is thus possible to rewrite the integral using a nonlinear change of variable,

$$\mathcal{Z}(z) = \sigma \int_{-\infty}^z n(s) ds. \quad (46)$$

\mathcal{Z} is nothing but the optical depth of the current point. We thus perform the changes of variable $z_1 \rightarrow \mathcal{Z}_1 \equiv \mathcal{Z}(z_1)$ and $r_{12} \rightarrow \mathcal{R}_{12}$, where

$$\mathcal{R}_{12} \equiv \frac{\mathcal{Z}(z_1 + r_{12} \cos \theta_{12}) - \mathcal{Z}(z_1)}{\cos \theta_{12}}. \quad (47)$$

This change of coordinates is such that the Jacobian exactly compensates the $n(\mathbf{r}_1)n(\mathbf{r}_2)$ term in Eq. (45). This finally gives

$$\gamma_L^{(2)} = \int d\mathcal{Z}_1 d\mathcal{R}_{12} \frac{d\Omega_{12}}{4\pi} \exp\{-(\mathcal{Z}_1 + \mathcal{Z}_2 + \mathcal{R}_{12})\}, \quad (48)$$

where

$$\mathcal{Z}_2 \equiv \mathcal{Z}(z_2) = \mathcal{Z}_1 + \mathcal{R}_{12} \cos \theta_{12} \quad (49)$$

is the optical depth of the second scatterer.

In Eq. (48), the integration over \mathcal{Z}_1 and \mathcal{R}_{12} is restricted to values such that $0 \leq \mathcal{Z}_1, \mathcal{Z}_2 \leq b$. Equation (48) is thus identical to Eq. (16), which establishes the equality of the ladder double-scattering bistatic coefficients for a uniform and a nonuniform medium. The generalization to higher order of scattering is immediate. Indeed, one simply needs to perform

a change of variable for every vector joining two consecutive scatterers, such that the angular variables $\theta_{N-1,N}, \phi_{N-1,N}$ are not touched, but the distance is nonlinearly rescaled like

$$\mathcal{R}_{N-1,N} \equiv \frac{\mathcal{Z}(z_{N-1} + r_{N-1,N} \cos \theta_{N-1,N}) - \mathcal{Z}(z_{N-1})}{\cos \theta_{N-1,N}}. \quad (50)$$

With such a change of variables, the ladder bistatic coefficient for the nonuniform slab is mapped on the coefficient for the uniform slab with identical optical thickness.

For the crossed bistatic coefficient, the situation is slightly more complicated. Indeed, the rescaling of the relative distance between successive scatterers preserves the angular variables (i.e., the relative orientation between consecutive scatterers), but not the relative distance. It thus happens that the transverse displacement $(x_{N-1,N}, y_{N-1,N})$ will be mapped to $(\mathcal{X}_{N-1,N}, \mathcal{Y}_{N-1,N})$ with the same direction but a different length. For each pair of scatterers, the rescaling of the length is different, which means that there is no simple connection between $(x_N - x_1, y_N - y_1) = (x_2 - x_1, y_2 - y_1) + (x_3 - x_2, y_3 - y_2) + \dots + (x_N - x_{N-1}, y_N - y_{N-1})$ and $(\mathcal{X}_N - \mathcal{X}_1, \mathcal{Y}_N - \mathcal{Y}_1)$. Thus, the term $\cos[(\mathbf{k}_{\text{in}} + \mathbf{k}_{\text{out}}) \cdot (\mathbf{r}_N - \mathbf{r}_1)]$ in the crossed bistatic coefficient is not easily taken into account. However, at exact backscattering, $\mathbf{k}_{\text{in}} + \mathbf{k}_{\text{out}} = 0$ and the cosine is unity for all spatial configurations. In this case, the transverse variables are irrelevant and one gets for a nonuniform medium the same contribution than for a uniform medium. As a consequence, at exact backscattering, the bistatic coefficients at each order (including single scattering) are all equal for a uniform or nonuniform medium; the enhancement factors are thus equal in both cases.

The proof has been given for a scalar wave. However, its extension to an electromagnetic wave of arbitrary polarization scattered by either point-dipole scatterers or atomic scatterers is trivial. Indeed, the proof involves a nonlinear rescaling of the distance between consecutive scatterers, but fully preserves their relative angular orientation. Thus, the angular dependence of the scattering amplitude, and the orientation of the polarization, are not affected by the rescaling and the proof for scalar wave and isotropic scatterers remains valid.

The proof has been given for an incoming plane wave which uniformly illuminates the medium. For a nonuniform laser beam (such as a Gaussian beam), each contribution must be conveniently weighted by the laser amplitude, as explained in Sec. III D. The weights involve the transverse properties of the medium and are thus not invariant under the nonlinear rescaling, Eq. (50). Thus, the equality of the bistatic coefficients for a slab and a Gaussian slab does not hold for an incoming Gaussian laser beam. It will remain approximately valid only if the waist of the laser beam is much larger than the mean-free path.

If the enhancement factor of the CBS cone is not affected by a nonuniform density, the shape changes (see discussion above) and it is difficult to draw general conclusions or make explicit calculations. One can however make the following observations.

(a) Typically, $\mathcal{R}_{N-1,N}$ is of order unity that implies that $r_{N-1,N}$ is of the order of the local mean-free path. The total transverse displacement (x_{1N}, y_{1N}) will thus be the sum of individual displacements which may be of very different lengths, depending whether the path explores deep regions inside the medium—where the mean-free path is short — or stays in the outer layers—where the mean-free path is much larger.

(b) For double scattering, the first and second scattering events typically take place at optical depth of order unity. Thus the angular width of the double-scattering CBS cone will be of the order of $1/k\bar{\ell}$, where $\bar{\ell}$ is the mean-free path *at unit optical depth*. For a very thick medium, this takes place in the wings of the Gaussian describing $n(\mathbf{r})$ and $\bar{\ell}$ may be much larger than the mean-free path ℓ at the center of the sample. This means that the CBS cone may be much narrower than naively expected from ℓ .

(c) For higher scattering orders, a typical path will explore denser regions of the medium with shorter mean-free paths, resulting in a globally slower spread of the transverse displacement (compared to uniform density). Thus, the contributions of the higher orders of scattering to the CBS cone, which, for a uniform semi-infinite medium, decrease in intensity as $N^{-3/2}$ and whose width decrease as $N^{-1/2}$, will show the same decrease in intensity (see proof above) but a slower decrease of the width. Thus, the tip of the CBS cone, which has a celebrated triangular shape $(1 - a|\theta|)$ for a scalar wave or an electromagnetic wave scattered by point-dipole scatterers in the parallel polarization channels, will be rounded for a nonuniform medium.

(d) For atomic scatterers, the effect of the internal structure is to reduce the contribution of higher orders of scattering to the CBS cone. Thus, the rounding of the cone tip is already present for a uniform slab. The modification due to nonuniform density is thus expected to be small.

The numerical results presented in Sec. V show the relative importance of those various remarks.

B. Width of the CBS cone in nonuniform media

It is possible to get some interesting insight on the width and shape of the CBS cone using the Gaussian slab geometry. Using Eqs. (42) and (46), we obtain for the optical depth:

$$\mathcal{Z} = \frac{b}{2} \operatorname{erfc}\left(\frac{z}{\sqrt{2}r_0}\right), \quad (51)$$

where erfc denotes the error integral function [21] and b the optical thickness given by Eq. (20).

We now assume that the medium is optically thick, i.e., $b \gg 1$. The first scattering event will typically take place at optical depth \mathcal{Z} of the order of unity. For a thick medium, this is in the outer layers of the medium, where the density is still low and the mean-free path quite long. Using the asymptotic expression [21] $\operatorname{erfc}(x) \approx (1/\sqrt{\pi}|x|)\exp(-x^2)$ valid for $x \rightarrow -\infty$, one obtains that the first scattering event takes place around

$$\tilde{z} \approx -r_0 \left(\sqrt{2 \ln \frac{b}{\sqrt{2\pi}}} - \frac{\ln \sqrt{2 \ln \frac{b}{\sqrt{2\pi}}}}{\sqrt{2 \ln \frac{b}{\sqrt{2\pi}}}} \right). \quad (52)$$

At this point, the density of scatterers is

$$\tilde{n} \approx n_0 \frac{\sqrt{4\pi \ln \frac{b}{\sqrt{2\pi}}}}{b} \quad (53)$$

and the mean-free-path

$$\bar{\ell} \approx \frac{r_0}{\sqrt{2 \ln \frac{b}{\sqrt{2\pi}}}}. \quad (54)$$

The latter equation implies that, apart from a *logarithmic* correction, the mean-free path at the first scattering event is essentially equal to the size of the medium, much larger than the mean-free path at the center of the medium! For a semi-infinite uniform medium, the angular width of a CBS cone is of order of $1/k\ell$, with a prefactor depending on the scalar or vector nature of the wave and on the polarization channel. For a scalar wave or a vector wave in the parallel channel, the full width at half maximum (FWHM) is roughly $0.7/k\ell$. It results from the superposition of CBS cones whose intensity and width decrease with the scattering order N . The double-scattering contribution is ≈ 10 times broader.

For a Gaussian slab, it is thus reasonable to expect that the double-scattering contribution will be dominated by paths scattered at unit optical depth, and thus will have a FWHM of the order of few $1/k\bar{\ell}$. Higher orders of scattering will penetrate deeper inside the medium, and will thus feel a reduction of the local mean-free path. Compared to a uniform medium, the typical transverse excursion of a multiple scattering path will thus be reduced, and the width of the corresponding CBS cone increased. To estimate the importance of this effect, it is useful to study how fast the mean-free path varies. From the equality $\ell = 1/n(z)\sigma$, one gets

$$\frac{d\ell}{dz} = \frac{\sqrt{2\pi}}{b} \frac{z}{r_0} \exp\left(\frac{z^2}{2r_0^2}\right). \quad (55)$$

At unity optical depth and for large optical thickness, one finds, using Eq. (52)

$$\left| \frac{d\ell}{dz}(\tilde{z}) \right| \approx 1. \quad (56)$$

In other words, the local mean-free path varies significantly when the optical depth changes by one unit. This implies that for higher orders of scattering—deeper inside the medium—the transverse excursion is strongly reduced. Thus, the CBS cones arising from higher orders of scattering is not expected

to be significantly narrower than the double-scattering contribution.⁸ Thus, we predict that the width of the CBS cone for a Gaussian slab will be of the order of the double-scattering width and will be given by

$$\Delta\theta \approx \frac{\beta}{k\tilde{\ell}} \quad (57)$$

with β a numerical constant depending on the polarization channel, but typically between 1 and 2. Plugging Eq. (54) finally gives

$$\Delta\theta \approx \frac{\beta}{kr_0} \sqrt{2 \ln \frac{b}{\sqrt{2\pi}}} \quad (58)$$

or, using the mean-free path ℓ at the center of the medium,

$$k\ell\Delta\theta \approx \frac{\beta}{b} \sqrt{4\pi \ln \frac{b}{\sqrt{2\pi}}} . \quad (59)$$

For a uniform slab medium, this dimensionless product $k\ell\Delta\theta$ tends to a constant (of the order of 0.7 for scalar waves and electromagnetic waves scattered by point-dipole scatterers, in the parallel polarization channels) when the optical thickness tends to infinity. On the contrary, for a Gaussian slab, the CBS cone gets narrower, roughly as the inverse of the optical thickness. This is a very dramatic effect which—as far as we know—has never been reported, probably because standard CBS experiments use sharp interfaces and media with constant density.

The summary of our analysis of the Gaussian slab case is that we know exactly the enhancement factor of the CBS cone (see Sec. III A) and have an approximate prediction, Eq. (58), for its width.

Various remarks can be made as follows.

(i) The narrowing of the CBS cone is after all a rather trivial effect. It is because scatterers that contribute to the CBS signal stem from the external layers of the medium.

(ii) A similar width is expected for a scalar wave, in all polarization channels for a vector wave and point-dipole scatterers and even for atomic scatterers, although the enhancement factors can be very different. This is because the width for a Gaussian slab is dominated by double scattering, whose width and shape are similar in all cases.

(iii) For a Gaussian sphere with large optical thickness, the physics is essentially the same. Indeed, the CBS signal will essentially originate from the outer layers of the sphere where the mean-free path is very large. It is the longitudinal

variation of the density which is the major ingredient, not the transverse variations. The reduced transverse extension will certainly cut the very long scattering paths (which may escape transversely) but it is unlikely to strongly affect the CBS cone width. The approximate expression, Eq. (58), is thus expected to be valid for a Gaussian sphere, i.e., for our experimental conditions.

(iv) Similarly, for a sphere with uniform density and large optical thickness, we expect that the CBS cone will be dominated by the interface. Cone widths slightly larger but comparable to the widths for a slab medium are thus expected.

(v) Equation (58), valid also for a Gaussian sphere, seems to suggest that the width of the CBS cone is nothing but—apart from a logarithmic correction—the diffraction angle associated with the scattering medium. This interpretation is definitely *incorrect*. It is not the transverse dimension that determines the CBS cone width, but the longitudinal variation of the density. The best proof is that the width is only weakly affected when the transverse size increases toward infinity (toward a Gaussian slab), see numerical results in Sec. V.

V. RESULTS

In this section, we present various results of Monte Carlo simulations using either scalar or electromagnetic waves, in the latter case either with point-dipole or atomic scatterers. The goal of these calculations is to explore the influence of the geometrical properties of the scattering medium on the CBS signal, and to test the qualitative ideas and quantitative approximations introduced above. The emphasis is put on the Gaussian sphere geometry, which is the one used in the experiments. We also report new experimental results on point-dipole and atomic scatterers, and compare them with the results of our Monte Carlo calculations.

A. Scalar wave

Scalar waves and isotropic scatterers are especially simple, because they allow to concentrate on effects purely due to the geometry of the medium, leaving aside the complications introduced by the polarization channels and the internal degree of freedom of atomic scatterers.

Figure 2 shows the enhancement factor α computed numerically as a function of the optical thickness b of the medium, for various geometries. The enhancement factor is defined as the ratio of the average intensity scattered in the exact backward direction to the average intensity scattered close to the backward direction, but outside the CBS cone. It is related to the bistatic coefficients through

$$\alpha = \frac{\gamma_L + \gamma_C(\theta=0)}{\gamma_L} \quad (60)$$

with the convention that the single-scattering contribution γ_S is included in the ladder contribution γ_L . For scalar waves or electromagnetic waves scattered by point-dipole scatterers in the parallel channels, the reciprocity theorem implies that $\gamma_C(\theta=0) + \gamma_S = \gamma_L$ [10] and thus

⁸If $|d\ell/dz|$ is much smaller than unity, the medium is locally uniform and a diffusion approximation (with a slowly varying diffusion constant) can be used. If $|d\ell/dz|$ is much larger than unity, on the contrary, an abrupt approximation could be used with a sharp interface at the entrance in the medium. For a Gaussian density, it turns out that neither the diffusion, nor the abrupt approximation can be used. This phenomenon is accidental for Gaussian density and no deep physics is hidden behind it.

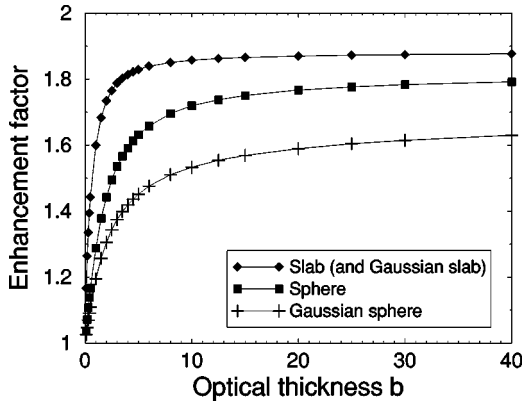


FIG. 2. Enhancement factor [as defined in Eq. (60)] of the CBS cone for a scalar wave scattered by point isotropic scatterers, for various geometries of the medium, as a function of the optical thickness b . It is significantly smaller for a Gaussian sphere—the geometry used in experiments on cold atoms—than for a slab, because long scattering paths are cut, which increases the relative weight of single scattering.

$$\alpha = 2 - \frac{\gamma_S}{\gamma_L}. \quad (61)$$

We numerically checked that the enhancement factors for the slab and Gaussian slab geometries are equal for any b , as proved in Sec. III C. For small b , the enhancement factor goes to unity in all geometries. This is due to single scattering that is dominant at small b and does not contribute to the CBS signal. The enhancement factor increases with b and saturates to a constant value as $b \rightarrow \infty$. For the slab geometry, we checked that the numerical results agree perfectly with the prediction of Ref. [22] obtained by numerically solving the Milne equation. For example, the saturation value at $b = \infty$ is 1.88, limited by single scattering. In the other geometries, the saturation value [and more generally, the full curve $\alpha(b)$] is lower, as these geometries reduce the weights of the long scattering paths (the photon exits more easily in the transverse directions). In all cases, the limiting value at $b = \infty$ is reached rather slowly—with a $1/b$ behavior—because γ_L contains significant contributions from very long paths that are cut at finite b . The most important conclusion which can be drawn from this figure is that the enhancement factor can be strongly reduced by purely geometrical effects, for example from 1.8 to 1.4 at $b=4$ when going from a slab to a Gaussian sphere geometry.

Figure 3 shows the width $\Delta\theta$ (FWHM) of the CBS cone (normalized with respect to $1/k\ell$, where k is the wave vector of the light and ℓ the mean-free path *at the center of the sample*), as a function of the optical thickness b for various geometries. Note that both axes are plotted in logarithmic scales. One can see that in all situations the product $k\ell\Delta\theta$ decreases with increasing optical thickness. Indeed, at fixed mean-free path, increasing b means increasing the sample size, which increases the relative proportion of long scattering paths. Those yield narrow cones, thus the total CBS cone gets narrower. For uniform (i.e., constant density of scatterers) geometries, the CBS cone gets narrower at increasing b

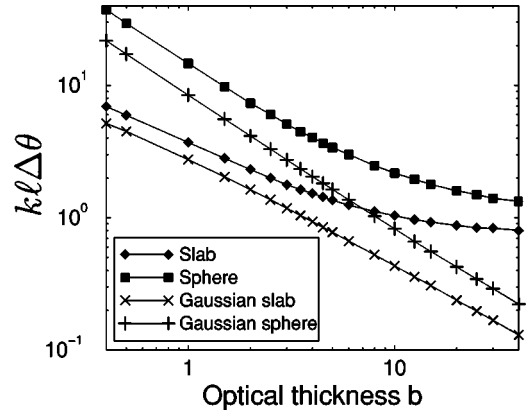


FIG. 3. Normalized width $k\ell\Delta\theta$ of the CBS cone for a scalar wave scattered by point isotropic scatterers, for various geometries of the medium; k is the wave vector of the light, ℓ the mean-free path at the center of the sample, and $\Delta\theta$ the full angular width at half maximum (FWHM) of the CBS cone. For the slab and sphere geometries—where the density of scatterers and consequently the mean-free path are constant across the sample—it decreases toward a constant value of the order of unity as $b \rightarrow \infty$. On the contrary, for the Gaussian slab and the Gaussian sphere, it continues to decrease quickly with increasing b , roughly like $1/b$. This is due to the multiple scattering in the external layers of the medium, where the mean-free path is much larger than the mean-free path at the center of the sample. Note the double logarithmic scale.

and saturates around $k\ell\Delta\theta \approx 1$ as $b \rightarrow \infty$. On the contrary, for Gaussian geometries, the cone width continues to decrease quickly even at large b , roughly like $1/b$. This agrees with the qualitative prediction of Sec. III C and is due to the multiple scattering in the external layers of the medium, where the local mean-free-path $\ell(\mathbf{r})$ is much larger than the mean-free-path ℓ at the center of the sample. We also note that this phenomenon is similar for the Gaussian slab and the Gaussian sphere, which proves that it is *not* due to the reduction of the transverse dimension of the scattering medium, but a consequence of the nonuniform density in the *longitudinal* direction.

A quantitative test of the theory developed in Sec. IV B is presented in Fig. 4, where we plot the product $bk\ell\Delta\theta$ versus b , using now linear scales. In other words, we multiply the data of Fig. 3 by b in order to compensate for the principal $1/b$ decrease. For the two Gaussian geometries, we observe that $bk\ell\Delta\theta$ increases slowly with b for the Gaussian slab and the Gaussian sphere geometries. The asymptotic expression, Eq. (59), predicts a $\sqrt{\ln(b)}$ increase at large b , but suffers from an unphysical singularity for small b . For the Gaussian slab—the medium for which the theory is done—the numerical calculation shows that the product $bk\ell\Delta\theta$ goes to zero as $b \rightarrow 0$. We thus regularize the logarithmic asymptotic behavior using

$$k\ell\Delta\theta \approx \frac{\beta}{b} \sqrt{2\pi \ln\left(1 + \frac{b^2}{2\pi}\right)}. \quad (62)$$

This function is plotted (for $\beta=1$) in Fig. 4. It reproduces the observed behavior, especially the slow logarithmic in-

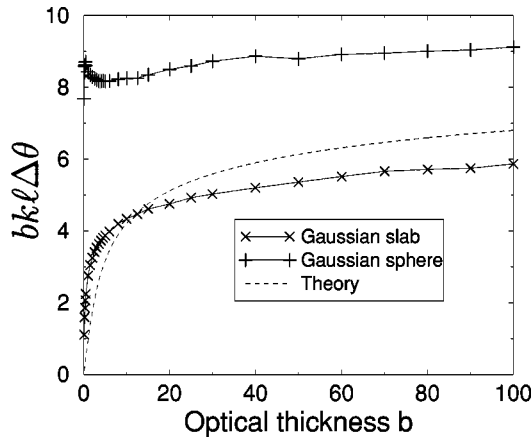


FIG. 4. Same data as in Fig. 3, but multiplied by b in order to compensate for the global $1/b$ decrease. The product $b k l \Delta \theta$ is approximately constant for the Gaussian slab and Gaussian sphere geometries, which implies that the CBS cone gets narrower roughly like the inverse of the optical thickness. The dashed line is the (regularized with $\beta=1$) prediction at large b , Eq. (62), which displays a logarithmic increase at large b , in agreement with the numerical result for a Gaussian slab and, to a lesser extent, for a Gaussian sphere. The fluctuations in the curves are due to a too small sampling in the Monte Carlo calculation.

crease at large optical thickness. Note, however, that the numerical result increases slightly more slowly than the prediction of Eq. (62). The reason is that we here use a constant β parameter. β is supposed to model the width of the CBS cone (in units of $1/k\ell$) for a uniform medium. From Fig. 3, such a width is clearly much larger than unity for thin slab and sphere media. Thus, the product $b k l \Delta \theta$ for a Gaussian sample results from the combination of the logarithmic increase in Eq. (62) and the slow decrease of β with b . At large b , the logarithmic divergence overcomes but, at moderate b , they more or less compensate, yielding an almost constant value. This is especially true for the Gaussian sphere, where β apparently varies more rapidly with b —see the slab and sphere curves in Fig. 3—and the logarithmic increase is very slow even at $b=100$. Altogether, for realistic optical thicknesses of a Gaussian sphere, the product $b k l \Delta \theta$ can be considered as almost constant, which means that the CBS cone itself gets narrower as the inverse of the optical thickness.

It is instructive to compare the angular width of the CBS cone with the so-called diffraction limit. Indeed, when illuminated by a plane wave with wave-vector k , a Gaussian sphere will—in the thin medium limit—diffract the initial wave producing a Gaussian diffraction figure at infinity whose angular width is given by

$$k r_0 \Delta \theta_{\text{diffraction}} = 2 \sqrt{\ln 2}, \quad (63)$$

which gives

$$b k l \Delta \theta_{\text{diffraction}} = \sqrt{8 \pi \ln 2} = 4.17. \quad (64)$$

It could thus be thought that the angular width of the CBS cone is nothing but the diffraction limit of the sample. However, this is not true. Indeed, as shown above, the width of

the CBS cone is imposed by the *longitudinal* variations of the mean-free path, whereas the diffraction limit is due to the *transverse* variations of the density. For a Gaussian sphere, they are of the same order of magnitude, hence a confusion is possible. Note first that the width of the CBS cone has a logarithmic increase at large b , which is absent in the diffraction limit, and second that the Gaussian slab has the same dependence while no diffraction argument applies there as the medium is transversely infinite.

The numerically computed CBS cones themselves are shown in Fig. 5 for $b=100$ in the four geometries. Clearly, they behave differently depending whether the density of scatterers is uniform or not. For the uniform slab and sphere geometries, the cone is relatively broad, but spiky at exact backscattering. This is a distinct signature of scattering at very large orders (contribution of very long scattering paths). On the contrary, for Gaussian geometries, the CBS cone is much narrower (typically 50 times narrower for $b=100$), as discussed above, and the top is rounded. As we have proved that, for a Gaussian slab, the contributions of the various scattering orders are identical to the slab situation, this is not due to a reduction of scattering at large orders. It is rather that long scattering paths go deeply inside the Gaussian medium and explore regions, where the mean-free path is significantly reduced. This slows down the transverse transport and kills the narrowing of the contributions with the order N of scattering. The contributions at various N have similar widths (instead of the $1/\sqrt{N}$ decrease for a uniform medium), leading to a overall smooth CBS cone.

B. Vector wave and point-dipole scatterers

We now turn to the results obtained for a vector wave scattered by point-dipole scatterers. As discussed above, the polarization channel is a crucial parameter. Parallel channels are expected to behave similarly to a scalar wave while, in perpendicular channels, very long scattering paths should play a minor role, leading to less intense and broader CBS cones.

Figure 6 shows the enhancement factor in the $lin \parallel lin$ channel as a function of the optical thickness, for various geometries. Again, it is identical for the slab and Gaussian slab geometry. A comparison with Fig. 2 immediately shows that CBS in this channel behaves qualitatively like CBS for a scalar wave, with an enhancement factor increasing with b up to a saturation value below 2 (because of single scattering), depending on the geometry. In the $h \parallel h$ channel, there is no single scattering, so that the enhancement factor of an incoming plane wave is equal to 2, for all geometries. This is because pairs of time-reversed scattering paths always have the same amplitude, leading to perfect contrast of the interferences.

The enhancement factor in the $lin \perp lin$ channel is shown in Fig. 7, for various geometries. At small b , the CBS signal is dominated by double scattering (single scattering is zero in this channel), for which the ladder and crossed contributions are equal. Thus, the enhancement factor is close to 2. For multiple-scattering beyond second order, the amplitudes of a pair of time-reversed paths are no longer equal, which im-

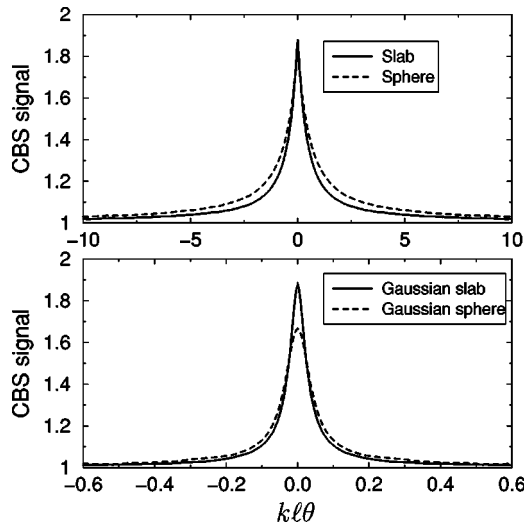


FIG. 5. The CBS cones numerically computed for optical thickness $b=100$ and various geometries. The cone is relatively broad and spiky for geometries with uniform density of scatterers, but narrow and smooth for the Gaussian geometries (note the different horizontal scales). The two latter features confirm that the CBS cone in Gaussian geometries are due to multiple scattering in the external layers of the medium, where the mean-free path is large and decreases rapidly with the optical depth.

plies a decrease of the crossed (interference) contribution and finally to a rather small enhancement factor as $b \rightarrow \infty$. Note that the rather large enhancement factor (1.6) observed in the $lin \perp lin$ channel for CBS by a cloud of Sr atom [18] is obtained in the regime of rather small b ($=2$ in the experiment), where double scattering is dominant. Cold Sr atoms behave like point-dipole scatterers when exposed to a laser beam quasiresonant with the resonance $J=0 \rightarrow J'=1$ line.

In the other perpendicular channel, $h \perp h$, the enhancement factor, shown in Fig. 8, is small for small b , because single scattering is important, but also rather small at large b because the pair of time-reversed paths which interfere has unbalanced amplitudes. However, in an intermediate regime,

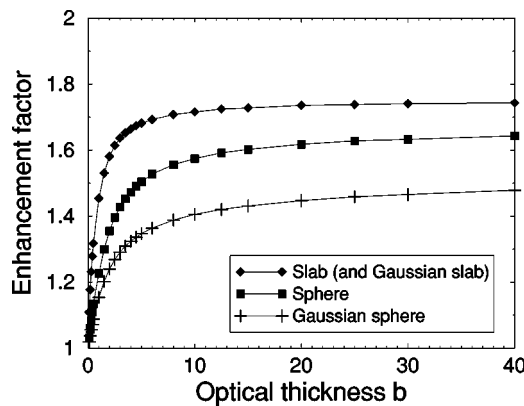


FIG. 6. Enhancement factor [as defined in Eq. (60)] of the CBS cone for a vector wave scattered by point-dipole scatterers in the $lin \parallel lin$ channel, for various geometries of the medium, as a function of the optical thickness b . It behaves very similarly to scalar waves, see Fig. 2.

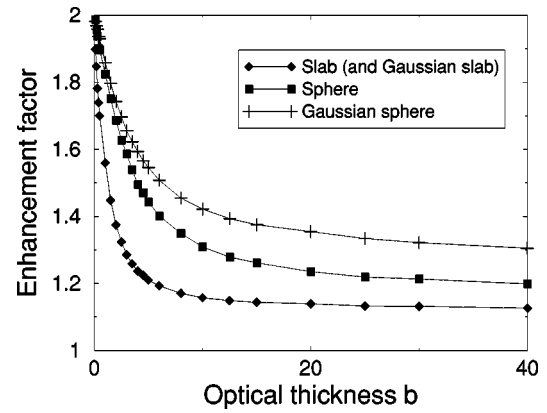


FIG. 7. Enhancement factor [as defined in Eq. (60)] of the CBS cone for a vector wave scattered by point-dipole scatterers in the $lin \perp lin$ channel, for various geometries of the medium, as a function of the optical thickness b . It is close to 2 at small b where double scattering dominates and decreases toward rather small values when $b \rightarrow \infty$.

double-scattering—for which the interfering amplitudes are equal—plays an important role while large order scattering is still fairly small. This results in a maximum of the enhancement factor for b around few units; the precise position of the maximum as well as the maximum enhancement factor depends on the geometry. Altogether, the $h \perp h$ is the least favorable one for the observation of CBS by point-dipole scatterers.

We have also calculated the width of the CBS cone in the various geometries. It is essentially the same for all polarization channels, and very similar to the data displayed in Fig. 3 for a scalar wave. For example, the results for the $h \parallel h$ channel (not shown) are almost indistinguishable from the scalar wave simulation on a double logarithmic scale (difference of the order of 10%). The results for the $h \perp h$ channel are displayed in Fig. 9, on a double logarithmic scale. In the uniform geometries (slab and sphere), the width decreases with increasing b until toward a asymptotic value $k\ell\Delta\theta$ of the order of 5. In the nonuniform channels (Gaussian slab and Gaussian sphere), $k\ell\Delta\theta$ continues to decrease as $b \rightarrow \infty$, roughly like $1/b$. The only noticeable difference with the scalar wave, Fig. 3, is that the saturation value at $b = \infty$ is significantly (about 6 times) larger than for a scalar wave. The reason is that, in such a nonreciprocal channel, the contribution of high-order scattering is very small and the width is essentially given by the double scattering contribution, without the narrowing effect due to higher-orders observed in the parallel channels. In Fig. 10, we plot the product $b k \ell \Delta \theta$ versus the optical thickness, on a linear scale, together with the analytic prediction, Eq. (62). Similarly to the scalar wave, one can clearly observe the logarithmic increase at large b , both for the Gaussian slab and the Gaussian sphere. The agreement with the prediction is even better than for the scalar wave. This is most probably because, in this nonreciprocal channel, the CBS cone in the slab geometry does not narrow significantly with increasing b (because high-scattering orders weakly contribute) and the pure loga-

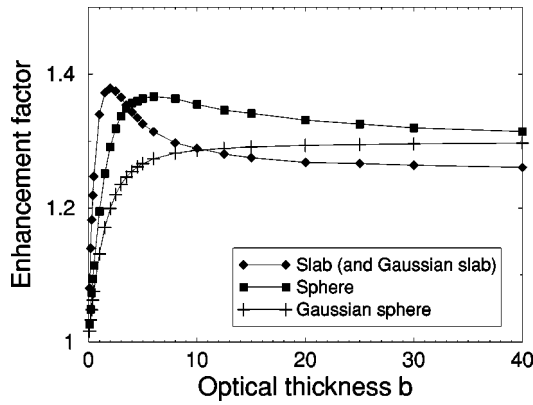


FIG. 8. Enhancement factor [as defined in Eq. (60)] of the CBS cone for a vector wave scattered by point-dipole scatterers in the $h\perp h$ channel, for various geometries of the medium, as a function of the optical thickness b . It is small both for small b (where single-scattering dominates) and for large b (where high-order scattering dominates), and present a maximum for optical thickness of few units.

rithmic increase expected for the double-scattering contribution is thus more visible.

In the linear channels, the situation is slightly more complex because the CBS cone does not have an azimuthal symmetry around the backscattering direction. In the $lin\parallel lin$ channel, it is rather anisotropic and two widths can be measured, a large one in the direction parallel to the polarization axis and a small one perpendicular to it [6]. Similarly, in the $lin\perp lin$ channel, the CBS cone has a four-fold symmetry and 2 widths can be measured, either parallel to the incoming

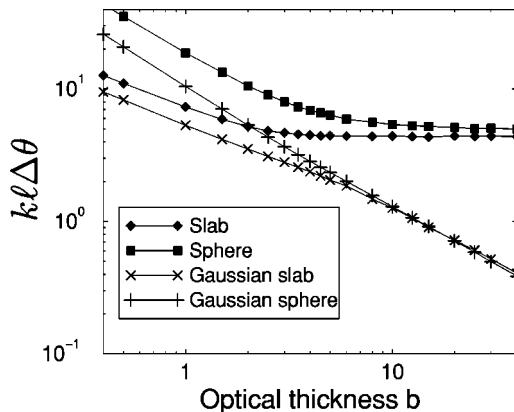


FIG. 9. Normalized width $k\ell\Delta\theta$ of the CBS cone for a vector wave in the $h\perp h$ channel, scattered by point-dipole scatterers, for various geometries of the medium; k is the wave vector of the light, ℓ the mean-free path at the center of the sample, and $\Delta\theta$ the full angular width at half maximum (FWHM) of the CBS cone. For the slab and sphere geometries—where the density of scatterers and consequently the mean-free path are constant across the sample—it decreases toward a constant value of the order of 5 as $b\rightarrow\infty$. On the contrary, for the Gaussian slab and the Gaussian sphere, it continues to decrease quickly with increasing b , roughly like $1/b$. This is due to the multiple scattering in the external layers of the medium, where the mean-free path is much larger than the mean-free path at the center of the sample. Note the double-logarithmic scale.

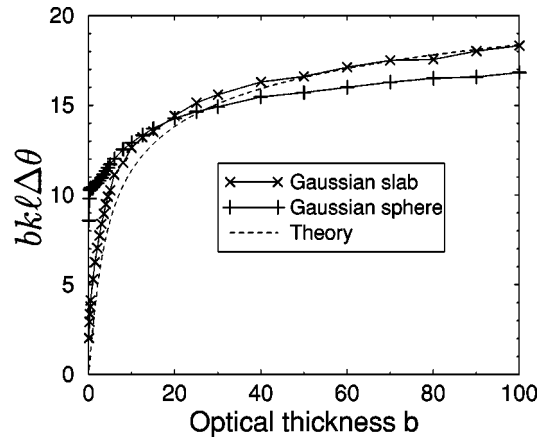


FIG. 10. Same data as in Fig. 9, but multiplied by b in order to compensate for the global $1/b$ decrease. The dashed line is the (regularized with $\beta=2.7$) prediction at large b , Eq. (62), which displays a logarithmic increase at large b , in agreement with the numerical result for a Gaussian slab and a Gaussian sphere.

or outgoing polarization, or at 45° from it [23]. We have studied the product $bk\ell\Delta\theta$ as a function of the optical thickness in the Gaussian sphere geometry for various polarization channels (and for scalar waves) and found that all the widths are very similar (within a factor 2 at most) and follow the logarithmic increase predicted by Eq. (62). As explained above, the perpendicular channels follow more closely this logarithmic increase because high scattering orders contribute less. However, it remains true that the most important effect is the narrowing effect due to scattering in the external layers of the cloud. This proves that the CBS cone in such a geometry is essentially dominated by low-order multiple scattering in the external layers of the sample.

The CBS cones themselves, calculated for $b=100$ and various geometries are shown in Figs. 11 and 12, in the $h\parallel h$ and $h\perp h$ channels, respectively. In the $h\parallel h$ channel, where the enhancement factor is equal to 2, the cone shapes are very similar to those obtained for a scalar wave, see Fig. 5: they are broad and spiky in the uniform geometries and narrow and smooth in the Gaussian geometries, as expected from the discussion in Sec. V A. In the $h\perp h$ channel, the situation is different: the cones are significantly broader than in the $h\parallel h$ channel and smooth in the four geometries. This is because pairs of long time-reversed scattering paths have typically unbalanced amplitudes and thus contribute little to the CBS interference.

In Fig. 13, we show the CBS cone experimentally observed on a suspension of TiO_2 particles. The particles are sufficiently small so that they behave like point-dipole scatterers [9]. The scattering medium is a slab of very large optical thickness, almost a semi-infinite medium. In the $h\parallel h$ channel, we observe an enhancement factor of 1.92, while the standard prediction is a factor 2. The Monte Carlo calculation, also shown in the figure as a dotted line, is done with an optical thickness $b=100$, but it is almost indistinguishable from the cone obtained for larger b values. The computed curve agrees remarkably well with the experimental observation, even in the far wings of the cone. The only

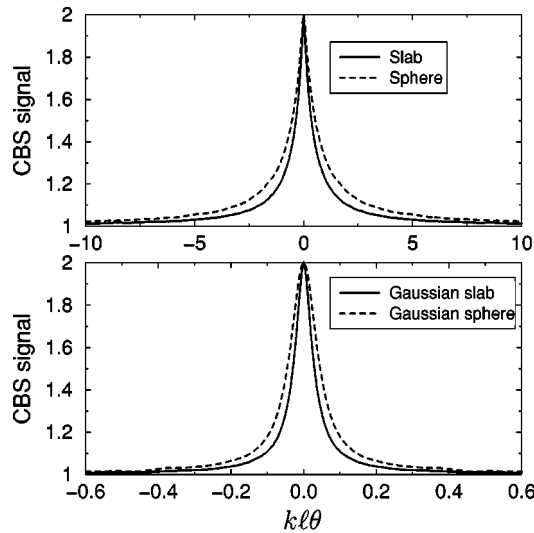


FIG. 11. The CBS cones numerically computed for optical thickness $b=100$ and various geometries, in the $h\parallel h$ channel. The cone is relatively broad and spiky for geometries with uniform density of scatterers, but narrow and smooth for the Gaussian geometries. The two latter features confirm that the CBS cone in Gaussian geometries are due to multiple scattering in the external layers of the medium, where the mean-free path is large and decreases rapidly with the optical depth.

noticeable difference is near the tip of the cone, see the inset in the figure. Three effects may explain this difference: first, the finite resolution of the optical apparatus used for the analysis of the CBS cone (of the order of 0.1 mrad) certainly rounds the top of the tip. Second, the finite transverse extension of the incoming laser beam induces, as shown in Sec. III D an imbalance of the amplitudes of the time-reversed scattering paths which interfere. In the specific case of a slab geometry (as used in our experiment) exposed to a Gaussian

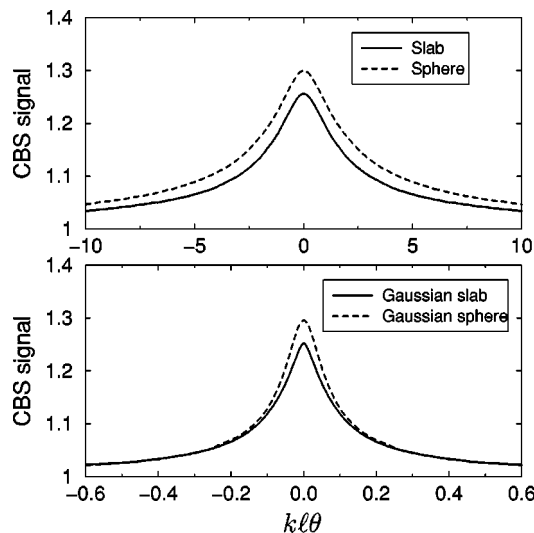


FIG. 12. Same as Fig. 11, but in the $h\perp h$ channel. The cones are less intense, slightly broader, and smoother for the uniform geometries. This is because the interference contrast of long scattering paths is very small in this channel.

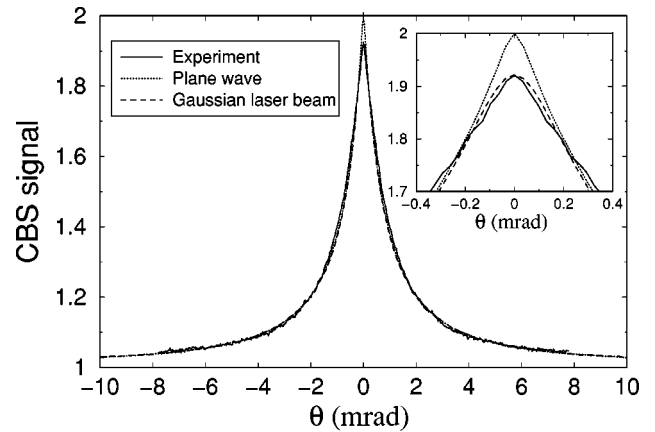


FIG. 13. The CBS cone observed experimentally on a slab of TiO_2 particles with very large optical thickness, in the $h\parallel h$ channel. It is compared with a Monte Carlo calculation using either an incoming plane wave (dotted line; in this case, the enhancement factor is exactly 2) or a Gaussian plane wave, which can be exactly taken into account through convolution with a Gaussian. Even if the incoming laser beam has a large waist (in the present case, the FWHM of the laser intensity is 32 times the mean-free path), it induces a significant decrease of the enhancement factor and a rounding of the cone tip. The agreement with the experimentally observed cone is excellent.

laser beam, this can be exactly taken into account through a convolution of the signal with the angular distribution of the laser beam. Third, the imperfections in the optics are responsible for a contamination of the $h\parallel h$ by the $h\perp h$ channel. As the latter channel has a small enhancement factor (and a large contribution of single scattering), the net effect is a reduction of the enhancement factor, estimated here to be of the order of few percents. The first two effects can be taken into account by convolving the CBS cone for a plane wave by a Gaussian (or similarly doing the calculation for a Gaussian laser beam with proper angular width). We show such a calculation as a dashed line in Fig. 13. It reproduces almost perfectly the observed CBS cone. This gives us confidence that the experimental setup is adequate for the observation of CBS; the same optical apparatus is used for observation of the CBS cone on a cloud of cold Rb atoms. This gives us also confidence that the Monte Carlo method used is reliable. In Fig. 14, we plot the experimentally measured angular width of the CBS cone as a function of the optical thickness. The experimental data are obtained by varying the geometrical thickness of the sample while keeping constant the density of scatterers and consequently the mean-free path. The experimental curve behaves as predicted by the Monte Carlo simulation: it decreases when the optical thickness increases and saturates to a constant value as $b\rightarrow\infty$. The agreement with the Monte Carlo calculation is very good. Note however that the Monte Carlo calculation does not include the effect of the liquid in which the TiO_2 particles are in suspension. Thus, the computed curves (i.e., the effective thickness of the sample) are rescaled in order to take into account—in a very approximate way—this effect. It is thus not surprising that some deviation is observed at small b .

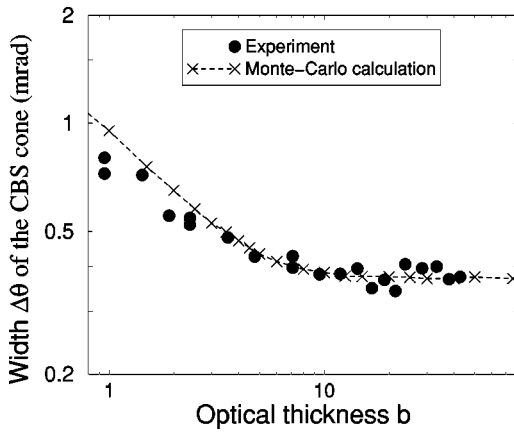


FIG. 14. Width of the CBS cone experimentally observed on a uniform slab of TiO_2 particles (in the $h\parallel h$ channel) as a function of the optical thickness b . It shows that the width decreases with the optical thickness, but slowly in the slab geometry, in accordance with the Monte Carlo calculation. This is in sharp contrast with the behavior observed on a cloud of cold atoms, see Fig. 18, where the width quickly decreases with b , an effect directly related to the nonuniform density of atoms. Note the double logarithmic scale.

C. Vector waves and atomic scatterers

In this section, we present experimental results as well as numerical calculations using a Monte Carlo method, for scattering of a vector wave (light) by a sample of cold Rb atoms. The frequency of the laser beam is chosen close to the $J=3 \rightarrow J'=4$ resonance line, see Sec. II. We assume that the initial atomic state is completely unpolarized and that inelastic transitions to other hyperfine levels are negligible. Both assumptions are likely to be valid in our experimental conditions.

In Ref. [24], we show a detailed analysis of the cone shape in the various channels. In the present paper, we rather concentrate on the influence of the optical thickness and the geometry of the medium.

We first show in Fig. 15 the computed CBS cone in the $h\parallel h$ channel and large optical thickness $b=100$ for various geometries. The comparison with the same plot for point-dipole scatterers, Fig. 11, shows dramatic effects: the enhancement factor is enormously reduced (from 2 to 1.05), the cones are slightly broader and the tip is rounded even in the slab and sphere geometries. This is a direct proof that the internal structure of the atoms is responsible for a strong reduction of interference effects even in the parallel polarization channels. It turns out that the cones in the figure are qualitatively similar to those observed for point-dipole scatterers in the $h\perp h$ channel (see Fig. 12), where interference effects are reduced because of the chosen polarization. From the figure, we also learn that the narrowing effect in the Gaussian geometries, discussed above for a scalar wave, equally applies for a cloud of cold atoms, where the CBS cone essentially arises from multiple scattering in the external layers of the cloud.

A careful analysis of the atomic scattering vertex [8,25,26] shows that indeed a small enhancement factor is expected in the $h\parallel h$ channel, but that the largest enhance-

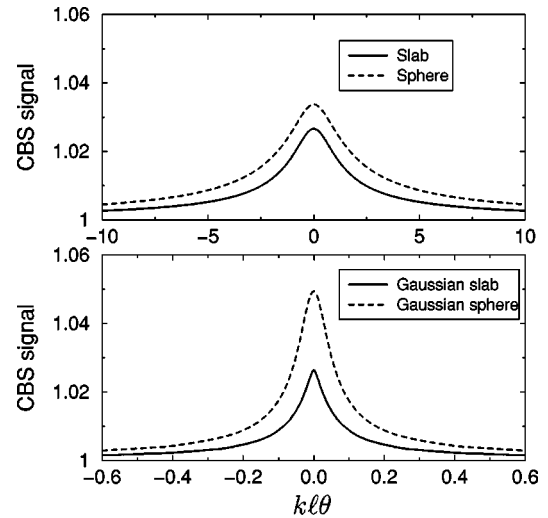


FIG. 15. The CBS cones numerically computed for Rb atoms with optical thickness $b=100$ and various geometries, in the $h\parallel h$ channel. The cone is smooth is all geometries, like in the $h\perp h$ channel for point-dipole scatterers, relatively broad for geometries with uniform density of scatterers, but narrow for the Gaussian geometries. This again confirms that the CBS cone in Gaussian geometries is due to multiple scattering in the external layers of the medium, where the mean free-path is large and decreases rapidly with the optical depth.

ment factor is expected in the $h\perp h$ channel. This is surprising, because it is the worst channel for point-dipole scatterers. The experimental results [5,6] as well the numerical calculations published elsewhere [24] fully confirm this unexpected behavior.

Figure 16 shows the measured CBS cone in the $h\perp h$ polarization channel at $b=19$ (detuning= 0.43Γ) and its comparison to a Monte Carlo simulation performed with the experimentally measured parameters for the atomic cloud and the laser beam. We performed two different calculations, using for the density of scatterers either a Gaussian function (this is the Gaussian sphere geometry) or an $\exp(-r^4/r_0^4)$ density [which we will note “ $\exp(-r^4)$ ” geometry]. There is no adjustable parameter. The 2D images obtained from the CCD are angularly averaged to improve signal-to-noise (this is safe since the cone is isotropic in the circular polarization channels). As one clearly sees, the experimental cone shape is intermediate between the two computed ones. This is not really surprising as the experimentally measured density is a bit sharper than a Gaussian—see the plot in Fig. 1—but less sharp than $\exp(-r^4/r_0^4)$. The experimentally measured angular width (0.72 mrad) is half-way between the computed angular widths for the Gaussian sphere geometry (0.54 mrad) and the $\exp(-r^4)$ geometry (0.90 mrad).

Next we study the angular width of the cone (obtained in the $h\perp h$ channel) as a function of the optical thickness. We measure the cone width (in mrad) as a function of the laser detuning. This is shown in Fig. 17 together with simulations in spherical geometries. All experimental points (full circles in the figure) correspond to cones recorded with the *same* atomic cloud, but for different laser detunings. We thus take advantage of the resonant scattering cross section of the at-

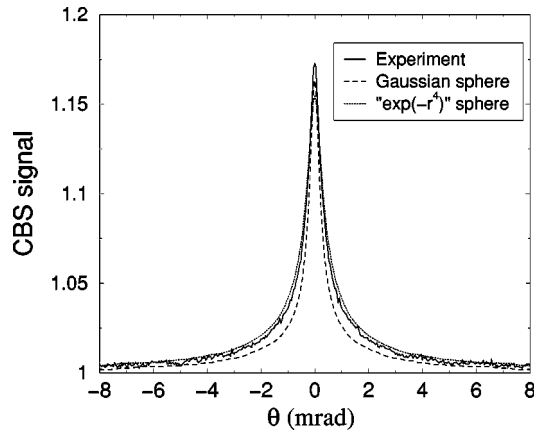


FIG. 16. The experimentally observed CBS cone on a cloud of cold rubidium atoms (optical thickness 19) in the $h \perp h$ channel, compared with the cone computed using a Monte Carlo method for a Gaussian sphere geometry and a $\exp(-r^4)$ geometry. The enhancement factor is well reproduced, as well as the shape. The angular width of the experimental cone is intermediate between those computed for the two geometries. This is probably because the density of the actual experimental medium is close to a Gaussian, but slightly sharper like the $\exp(-r^4)$ geometry.

oms to vary the optical thickness without changing the sample geometry. Although the mean-free-path ℓ varies roughly by a factor 65, one can see that the cone width changes at most by a factor 2.6. Under the same conditions, the cone width obtained for the uniform sphere changes by a factor 25. This is a strong signature of the effect of the inhomogeneous density in the sample. Indeed, Fig. 17 clearly

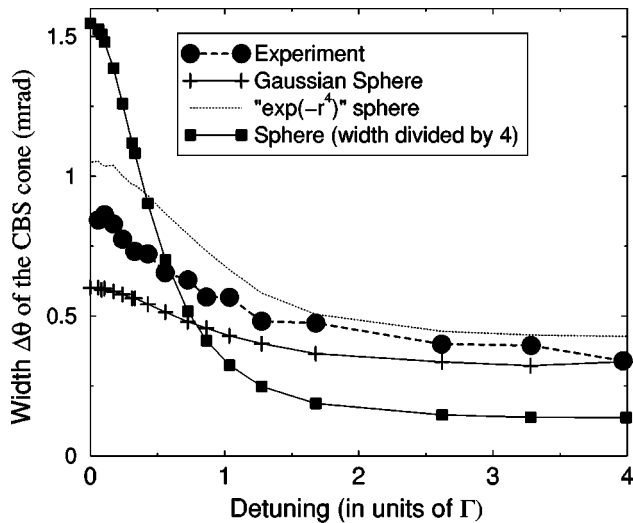


FIG. 17. Angular width (in mrad) of the atomic CBS cone in the $h \perp h$ channel, as a function of the detuning of the CBS probe beam. Note the small variation of the cone width (a factor 2.6) for the experiment and the inhomogeneous model geometries although ℓ is varied by a factor 65. The width obtained for the sphere geometry have been divided by 4 to appear on the same scale; its value as well as its dependence vs the optical thickness is completely incompatible with the experimental results. This clearly rules out the spherical geometry with uniform density.

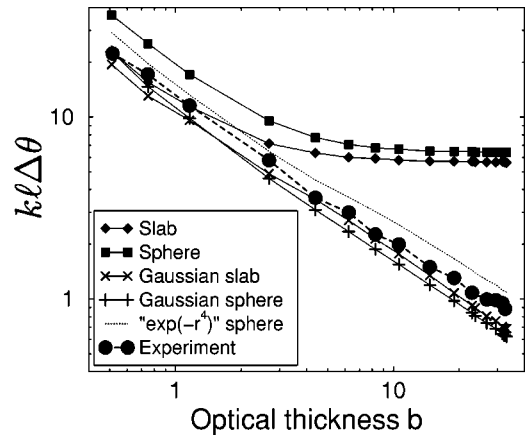


FIG. 18. Normalized width $k\ell\Delta\theta$ of the CBS cone for a vector wave in the $h \perp h$ channel, scattered by Rb atoms, for various geometries of the medium; k is the wave vector of the light, ℓ the mean-free path at the center of the sample, and $\Delta\theta$ the full angular width at half maximum (FWHM) of the CBS cone. For the slab and sphere geometries—where the density of scatterers and consequently the mean-free path are constant across the sample—it decreases toward a constant value of the order of 5 as $b \rightarrow \infty$. On the contrary, for the Gaussian slab and the Gaussian sphere, it continues to decrease quickly with increasing b , roughly like $1/b$, in complete similarity with a scalar wave or a vector wave scattered by point dipole scatterers, compare with Figs. 3 and 9. Note the double logarithmic scale. The experimental curve follows roughly a $1/b$ decrease, which shows that the dominant multiple-scattering events take place in the external layers of the atomic cloud, where the mean-free path is considerably larger than at the center.

shows that the experimental results are in excellent agreement with the predictions for a medium whose density varies smoothly [either a Gaussian sphere or a $\exp(-r^4)$ geometry] but are in complete disagreement with the prediction for a sphere of constant density.

The same data are used for Fig. 18, which shows the normalized CBS cone width $k\ell\Delta\theta$ measured in the $h \perp h$ channel as a function of the optical thickness [deduced from the laser detuning and the on-resonance value b_{res} through Eq. 2] at the center of the atomic cloud. A set of numerical predictions for different geometries is shown together with the experimental result. Their behaviors are similar to what is observed for a scalar wave, Fig. 3, and point-dipole scatterers, Fig. 9. In the uniform geometries, the width decreases with increasing b and saturates at $k\ell\Delta\theta \approx 5$ when $b \rightarrow \infty$. On the contrary, for Gaussian geometries, for the $\exp(-r^4)$ geometry and for the experimental results, it continues to decrease quickly, roughly like $1/b$. The experimentally observed behavior clearly follows the prediction for an inhomogeneous density, confirming the pertinence of the physical picture exposed before. Thus the width of the CBS cone in our experiment is *not* determined by the mean-free-path ℓ at the center of the cloud, but by the mean-free path *at unit optical depth*. As long as the width of the CBS cone is concerned, the most important effect is the smooth spatial variation of the mean free-path associated with the dominant multiple scattering events taking place in the external layers of the atomic cloud.

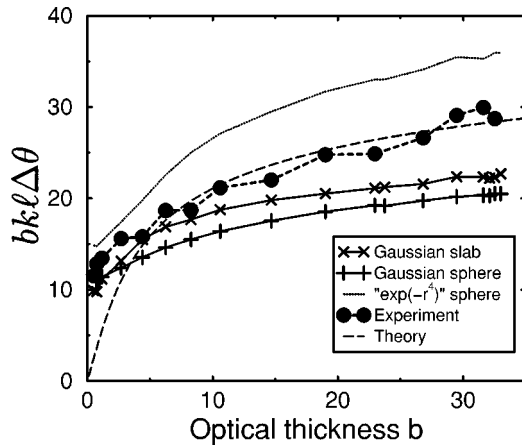


FIG. 19. Same data as in Fig. 18, but multiplied by b in order to compensate for the global $1/b$ decrease. The theory (dashed line) is the (regularized with $\beta=2.7$) prediction at large b , Eq. (62), which displays a logarithmic increase at large b , in agreement with the numerical result for a Gaussian slab and a Gaussian sphere. It follows remarkably well the experimental result. Note that, for a spherical density of the type $\exp(-r^4/r_0^4)$, the width is larger than the experimental result. This agrees with the fact that the experimental atomic density varies more sharply than a Gaussian, but less sharply than $\exp(-r^4/r_0^4)$.

When the $1/b$ decrease observed in Fig. 18 is compensated for, see Fig. 19, we again observe the logarithmic increase with b for the Gaussian geometries, in agreement with the theoretical prediction, Eq. (62). The experimental result itself follows very well the logarithmic prediction, which proves that our model catches the essential part of the physics of multiple scattering of light by a cloud of cold atoms. For the $\exp(-r^4)$ geometry, the theory developed above is not supposed to be valid as the derivation of the logarithmic term explicitly involves the shape of the density of scatterers. However, it does not lie too far from the result for the Gaussian sphere. This means—as explained in Sec. IV B—that the $1/b$ decrease of the width is a very general phenomenon for media, where the density varies smoothly. The edges of the $\exp(-r^4)$ geometry are sharper, that is closer to a sharp interface like in the sphere geometry; it is thus not surprising that the width is intermediate between the width for the Gaussian sphere and the width for the sphere. The same is valid for the experimental result, consistently with the observed density profiles that are sharper than a Gaussian function. Note also that all the observed widths are significantly larger than the “diffraction” limit, Eq. (64), which proves that they are due to longitudinal effects in the multiple-scattering phenomenon, and not to a trivial transverse effect.

We now turn to the CBS enhancement factor as a function of the optical thickness. In Fig. 20, we compare experimental results with Monte Carlo simulations for various atomic geometries. One clearly sees in the three spherical geometries as well as in the experiment, the initial increase of the enhancement factor with the optical thickness, followed by a drop at large b . The physical interpretation is clear: at small b (far from resonance), the medium is optically thin and single-scattering dominates, which kills the enhancement

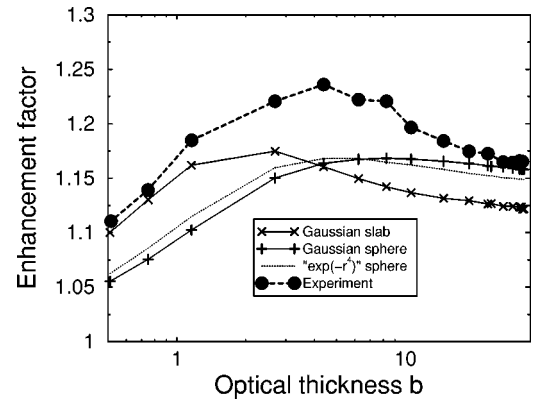


FIG. 20. Enhancement factor [as defined in Eq.(60)] of the CBS cone for a vector wave scattered by a cloud of rubidium atoms in the $h \perp h$ channel, for various geometries of the medium, as a function of the optical thickness b (in logarithmic scale). The Gaussian profile of the laser beam used in the experiment is taken into account in the simulations. The enhancement factor is small both for small b (where single-scattering dominates) and for large b (where high-order scattering dominates), and present a maximum for optical thickness of few units, where double (and low-order) scattering is most important. The experimental result follows the same behavior, although it is slightly but significantly larger. This discrepancy could be due to some residual optical pumping of the atoms by the CBS probe beam.

factor. As the optical thickness increases, the relative contribution of double-(and more generally low order of) scattering increases; as these short scattering paths have a rather high interference contrast, the enhancement factor increases. At large b , the long paths with small interference contrast come into play and the enhancement factor diminishes. The fact that, for the three geometries, a similar behavior is observed shows that the phenomenon is robust.

In all cases, the enhancement factor increases from 1 (at $b=0$) to a maximum value reached around $b=5$ then slowly decreases toward an asymptotic value when $b \rightarrow \infty$. In practice, the asymptotic value is reached above $b=20$. The agreement is, however, not perfect, the observed enhancement factor being systematically larger than the computed value. It is only in the asymptotic region $b \rightarrow \infty$ that the value 1.16 computed for the Gaussian sphere geometry is reached. We are not yet sure of the reason for this discrepancy. Some possibilities are as follows.

(i) Imperfections of the optical apparatus (in particular the quality of the incoming and detected polarization states). This can be ruled out: the largest enhancement factor is obtained in the $h \perp h$ channel, any optical imperfection is thus likely to decrease the observed value, not to increase it.

(ii) In the absence of the atomic cloud (no MOT), there is still some light scattered by various parts of the experimental setup that reach the detector. Most of this background is due to the dilute vapor of hot atoms filling the cell. This background, which represents less than 10% of the signal recorded in the presence of the atomic cloud, is subtracted before calculation of the enhancement factor. However, the contribution of the “hot” background may depend on the presence or not of the (optically thick) cloud of cold atoms.

This could lead to an overestimation of the enhancement factor by at most 0.01.

(iii) Non-Gaussian shape of the medium. Indeed, the experimentally recorded density profiles, Fig. 1, are far from perfectly Gaussian. We also computed in Fig. 20 the enhancement factor using a $\exp(-r^4/r_0^4)$ density profile in the medium, which reproduces more faithfully the rather sharp edges of the atomic cloud. Obviously, this does not suppress the discrepancy. Additionally, we have considered the case of an anisotropic Gaussian medium. We have calculated the CBS cone for $b=26$ with an anisotropy factor $3/2$ (plate shape) and $2/3$ (cigar shape) in the directions perpendicular to the incoming beam. This slightly modifies the width of the CBS cone (of the order of 20%) but alters only marginally the enhancement factor. If a different anisotropy factor is taken in the two directions perpendicular to the incoming beam, the CBS cone in the helicity channels loses its azimuthal symmetry. The experimentally recorded CBS cones in the $h \perp h$ channel are almost perfectly circular; we thus think that there is no significant transverse anisotropy. In summary, it is unlikely that deviation from a Gaussian shape of the medium is responsible for the discrepancy.

(iv) Stray magnetic field. It is known that even a rather small magnetic field (of the order of 1 G) modifies the properties of CBS [23]. However, it is unlikely that the atoms are exposed to more than 0.1 G in the experiment.

(v) Role of the other atomic transitions. Although the CBS probe beam is quasisonant with the $J=3 \rightarrow J'=4$ transition, there is a small probability that an atom scatters (elastically or not) a photon on another transition. Taking into account *inelastic* transitions to other ground-states (such as $J=3 \rightarrow J'=3 \rightarrow J''=2$) would be rather difficult in Monte Carlo calculations because then the propagator at various frequencies would have to be used. *Elastic* scattering, where the other accessible excited levels are probed ($J=3 \rightarrow J'=4, 3, 2 \rightarrow J=3$), could be treated along the lines described in this paper, as the full scattering amplitude is the coherent superposition of the contributions from the various J' states. Luckily, the detuning used in our experiment for the closest transition ($3 \rightarrow 3$) is always much larger (at least a factor 6) than the detuning for the $3 \rightarrow 4$ transition, so that the effect of other transitions on the CBS cone is likely to be small. This is supported by preliminary experimental results where the CBS enhancement factor was measured for both positive and negative detunings. A quantitative estimate, however, requires further studies [27].

(vi) Nonuniform distribution of the initial atomic state over the Zeeman sublevels. A basic assumption of our calculation is that the initial atomic state is completely depolarized, a reasonable assumption for atoms produced in a MOT. We cannot however exclude some residual polarization, even after the magnetic field of the MOT is switched off. This would affect the enhancement factor.

(vii) Optical pumping. The CBS probe beam is rather weak but, especially when it is circularly polarized, it may optically pump the atoms in a nonuniform distribution over the Zeeman sub-levels. This effect is difficult to estimate in optically thick media, because, except close to the entrance of the medium, the atoms are exposed not only to the incoming beam but mainly to the light scattered by other atoms. Recent experimental results [24] seem to indicate that, with a weaker probe beam, the discrepancy between the calculation and the experiment is reduced. We are thus inclined to think that optical pumping is the relevant phenomenon.

VI. CONCLUSION

We have presented in this paper both experimental and numerical results on coherent backscattering of light by a cloud of cold rubidium atoms. We have shown that the inhomogeneous density profile in the cloud plays a key role in determining the angular width of the CBS cone, in sharp contrast with what is observed for media with uniform density of scatterers. Especially, for a medium with a spherically symmetric Gaussian density, the properties of the CBS cone are essentially determined by the lowest orders of multiple scattering, when the photon is scattered in the outer layers of the cloud. Monte Carlo simulations which take fully into account the internal structure of the atoms correctly predict the CBS cone shape and angular width as well as the enhancement factor.

ACKNOWLEDGMENTS

We thank the CNRS and the PACA Region for financial support. We also thank the Groupe de Recherche PRIMA of CNRS. We gratefully acknowledge the important contribution of J.-C. Bernard to the development of the experiment. Laboratoire Kastler-Brossel de l'Université Pierre et Marie Curie et de l'École Normale Supérieure is Unité Mixte de Recherche 8552 du CNRS. CPU on a Cray SX5 computer has been provided by IDRIS.

-
- [1] E. Akkermans, P.E. Wolf, and R. Maynard, *Phys. Rev. Lett.* **56**, 1471 (1986).
 [2] R. Lenke and G. Maret, *Eur. Phys. J. B* **17**, 171 (2000).
 [3] E. Akkermans, P.E. Wolf, R. Maynard, and G. Maret, *J. Phys. (France)* **49**, 77 (1988); M.B. van der Mark, M.P. van Albada, and A. Lagendijk, *Phys. Rev. B* **37**, 3575 (1988); **38**, 5063 (1988).
 [4] R. Lenke and G. Maret, in *Scattering in Polymeric and Colloidal Systems*, edited by W. Brown (Gordon and Breach Sci-

ence Publishers, Reading, U.K., 2000), p. 1.

- [5] G. Labeyrie, F. de Tomasi, J.-C. Bernard, C.A. Müller, C. Miniatura, and R. Kaiser, *Phys. Rev. Lett.* **83**, 5266 (1999).
 [6] G. Labeyrie, C.A. Müller, D.S. Wiersma, Ch. Miniatura, and R. Kaiser, *J. Opt. B: Quantum Semiclassical Opt.* **2**, 672 (2000).
 [7] T. Jonckheere, C.A. Müller, R. Kaiser, C. Miniatura, and D. Delande, *Phys. Rev. Lett.* **85**, 4269 (2000).
 [8] C.A. Müller, T. Jonckheere, C. Miniatura, and D. Delande,

- Phys. Rev. A **64**, 053804 (2001).
- [9] D.S. Wiersma, M.P. van Albada, B.A. van Tiggelen, and A. Lagendijk, Phys. Rev. Lett. **74**, 4193 (1995).
- [10] B.A. van Tiggelen and R. Maynard, in *Wave Propagation in Complex Media*, edited by G. Papanicolaou, IMA Vol. 96 (Springer, New York, 1997), p. 252.
- [11] G. Labeyrie, C. Miniatura, and R. Kaiser, Phys. Rev. A **64**, 033402 (2001).
- [12] E.E. Gorodnichev, S.L. Dudarev, and D.B. Rogozkin, Phys. Lett. A **144**, 48 (1990).
- [13] M.C.W. van Rossum and T.M. Nieuwenhuizen, Rev. Mod. Phys. **71**, 313 (1999).
- [14] V.D. Ozrin, Waves Random Media **2**, 141 (1992).
- [15] E. Amic, J. Luck, and T. Nieuwenhuizen, J. Phys. I **7**, 445 (1997).
- [16] C.A. Müller and C. Miniatura, J. Phys. A **35**, 10163 (2002).
- [17] B. v. Tiggelen, Ph.D. thesis, University of Amsterdam, 1992 (unpublished); available at <http://tnweb.tn.utwente.nl/copsweb/theses.html>.
- [18] Y. Bidet *et al.*, Phys. Rev. Lett. **88**, 203902 (2002).
- [19] W.H. Press, S.A. Teukolsky, W.T. Vetterling, and B.P. Flannery, *Numerical Recipes in Fortran (or C)* (Cambridge University Press, Cambridge, 1992).
- [20] A. Lagendijk and B. van Tiggelen, Phys. Rep. **270**, 143 (1996).
- [21] M. Abramowitz and I.A. Stegun, *Handbook of Mathematical Functions* (Dover, New York, 1972).
- [22] M.P. van Albada, M.B. van der Markt, and A. Lagendijk, in *Scattering and Localization of Classical Waves in Random Media*, edited by P. Sheng (World Scientific, Singapore, 1990), p. 97.
- [23] G. Labeyrie, Ch. Miniatura, C.A. Müller, O. Sigwarth, D. Delande, and R. Kaiser, Phys. Rev. Lett. **89**, 163901 (2002).
- [24] G. Labeyrie, D. Delande, C.A. Müller, C. Miniatura, and R. Kaiser, Europhys. Lett. **61**, 327 (2003).
- [25] C.A. Müller, Ph.D. thesis, Universities of Munich/Nice-Sophia Antipolis, 2001 (unpublished), http://www.ub.uni-muenchen.de/elektronische_dissertationen/physik/Mueller_Cord.pdf.
- [26] E. Akkermans, C. Miniatura, and C.A. Müller, e-print cond-mat/0206298.
- [27] D.V. Kupriyanov, I.M. Sokolov, P. Kulatunga, C.I. Sukenik, and M.D. Havey, Phys. Rev. A **67**, 013814 (2003).